NAVAL POSTGRADUATE SCHOOL

MONTEREY, CALIFORNIA

THESIS

COMPARISON OF GALLIUM NITRIDE HIGH ELECTRON MOBILITY TRANSISTORS MODELING IN TWO AND THREE DIMENSIONS

by

William Alexander Gibson

December 2007

Thesis Advisor:	Todd R. Weatherford
Second Reader:	Andrew A. Parker

Approved for public release; distribution is unlimited

THIS PAGE INTENTIONALLY LEFT BLANK

REPORT DOCUMENTATION PAGE				*Form Approved OMB No. 0704-0188*
Public reporting burden for this collection of information is estimated to average 1 hour per response, including the time for reviewing instruction, searching existing data sources, gathering and maintaining the data needed, and completing and reviewing the collection of information. Send comments regarding this burden estimate or any other aspect of this collection of information, including suggestions for reducing this burden, to Washington headquarters Services, Directorate for Information Operations and Reports, 1215 Jefferson Davis Highway, Suite 1204, Arlington, VA 22202-4302, and to the Office of Management and Budget, Paperwork Reduction Project (0704-0188) Washington DC 20503.				
1. AGENCY USE ONLY *(Leave blank)*	**2. REPORT DATE** December 2007		**3. REPORT TYPE AND DATES COVERED** Master's Thesis	
4. TITLE AND SUBTITLE Comparison of Gallium Nitride High Electron Mobility Transistors Modeling in Two and Three Dimensions.			**5. FUNDING NUMBERS**	
6. AUTHOR(S) William Alexander Gibson				
7. PERFORMING ORGANIZATION NAME(S) AND ADDRESS(ES) Naval Postgraduate School Monterey, CA 93943-5000			**8. PERFORMING ORGANIZATION REPORT NUMBER**	
9. SPONSORING /MONITORING AGENCY NAME(S) AND ADDRESS(ES) N/A			**10. SPONSORING/MONITORING AGENCY REPORT NUMBER**	
11. SUPPLEMENTARY NOTES The views expressed in this thesis are those of the author and do not reflect the official policy or position of the Department of Defense or the U.S. Government.				
12a. DISTRIBUTION / AVAILABILITY STATEMENT Approved for public release; distribution is unlimited			**12b. DISTRIBUTION CODE**	

13. ABSTRACT (maximum 200 words)

This thesis looks at modeling Gallium Nitride (GaN) High Electron Mobility Transistor (HEMT) Semiconductors. The GaN device has potential future military use in the high power and high frequency operation replacing costly millimeter wave tubes. This would affect military radar systems, electronic surveillance systems, communications systems and high voltage power systems by providing smaller and more reliable devices to drive operation. This thesis looks at using diamond substrate to improve the thermal management of a HEMT device over that of a sapphire substrate. The improved thermal management should lead to improved operating characteristics and reliability. The HEMT device was modeled using Silvaco software package and compared to an actual device on sapphire substrate. The HEMT modeling was done in two and three dimension modeling software. The results of the software model showed the improved thermal characteristics of the HEMT device on the diamond substrate over that of the sapphire.

14. SUBJECT TERMS Gallium Nitride, HEMT, High Electron Mobility Transistor, Silvaco, ATLAS, modeling.			**15. NUMBER OF PAGES** 77
			16. PRICE CODE
17. SECURITY CLASSIFICATION OF REPORT Unclassified	**18. SECURITY CLASSIFICATION OF THIS PAGE** Unclassified	**19. SECURITY CLASSIFICATION OF ABSTRACT** Unclassified	**20. LIMITATION OF ABSTRACT** UU

NSN 7540-01-280-5500 Standard Form 298 (Rev. 2-89)
Prescribed by ANSI Std. 239-18

THIS PAGE INTENTIONALLY LEFT BLANK

Approved for public release; distribution is unlimited

COMPARISON OF GALLIUM NITRIDE HIGH ELECTRON MOBILITY TRANSISTORS MODELING IN TWO AND THREE DIMENSIONS

William A. Gibson
Lieutenant, United States Navy
B.S.A.S.T, Thomas Edison State College, 2002

Submitted in partial fulfillment of the
requirements for the degree of

MASTER OF SCIENCE IN ELECTRICAL ENGINEERING

from the

NAVAL POSTGRADUATE SCHOOL
December 2007

Author: William Alexander Gibson

Approved by: Todd R. Weatherford
Thesis Advisor

Andrew A. Parker
Second Reader

Jeffrey B. Knorr
Chairman, Department of Electrical and Computer Engineering

THIS PAGE INTENTIONALLY LEFT BLANK

ABSTRACT

This thesis looks at modeling Gallium Nitride (GaN) High Electron Mobility Transistor (HEMT) Semiconductors. The GaN device has potential future military use in the high power and high frequency operation replacing costly millimeter wave tubes. This would affect military radar systems, electronic surveillance systems, communications systems and high voltage power systems by providing smaller and more reliable devices to drive operation. This thesis looks at using diamond substrate to improve the thermal management of a HEMT device over that of a sapphire substrate. The improved thermal management should lead to improved operating characteristics and reliability. The HEMT device was modeled using Silvaco software package and compared to an actual device on sapphire substrate. The results of the software model showed the improved thermal characteristics of the HEMT device on the diamond substrate over that of the sapphire.

THIS PAGE INTENTIONALLY LEFT BLANK

TABLE OF CONTENTS

I. INTRODUCTION 1
A. BACKGROUND 1
B. RELATED RESEARCH 4
1. Summary of Previous Research 4
2. DARPA Wide Bandgap Semiconductor Technology Thrust I 5
3. Navy Research 6
C. OBJECTIVE 7
II. HIGH ELECTRON MOBILITY TRANSISTORS (HEMT) 9
A. HEMT FUNDAMENTALS 9
1. AlGaN/GaN HEMT 9
2. Two Dimensional Electron Gas (2DEG) 14
3. Piezoelectric and Spontaneous Polarization 16
4. Thermal Effects 17
B. UC BERKELEY DEVICE 18
1. Testing the UC Berkeley Device 18
2. Results from UC Berkeley Device 19
III. HEMT MODELING 21
A. MODELING HEMT ON SAPPHIRE 21
1. Model Design 21
2. Comparison to Results from UC Berkeley Device 29
3. Comparison of a 2D to 3D Model 33
B. MODELING HEMT ON DIAMOND 42
1. Changes to Model for Diamond Substrate 42
2. Comparison of Diamond and Sapphire Substrate 42
IV. CONCLUSIONS AND RECOMMENDATIONS 47
A. CONCLUSIONS 47
B. RECOMMENDATIONS 48
LIST OF REFERENCES 51
APPENDIX A. MATLAB CODE 53
APPENDIX B. DECKBUILD CODE FOR 2D MODEL 55
APPENDIX C. DECKBUILD CODE FOR 3D MODEL 57
INITIAL DISTRIBUTION LIST 59

THIS PAGE INTENTIONALLY LEFT BLANK

LIST OF FIGURES

Figure 1. Typical AlGaN/GaN HEMT From [11]. 9
Figure 2. Crystal structure of Wurtzite GaN From [7]. 10
Figure 3. Bending and strain due to different thermal expansion coefficients From [5]. 14
Figure 4. Band Diagram of AlGaN/GaN Heterojunction From [5]. 15
Figure 5. Sheet charge density based as a function of Al composition From [15]. 15
Figure 6. Spontaneous polarization for Wurtzite crystal From [18]. 17
Figure 7. Low field electron mobility for GaN donor concentrations $10^{16}/cm^3$ (solid) $10^{17}/cm^3$ (dashed) $10^{18}/cm^3$ (dashed dotted) From [20]. 17
Figure 8. SEM image of GaN HEMT From [8]. 18
Figure 9. Room temperature (300º K) I(A)-V curves for UC Berkeley device. 19
Figure 10. Current effects of temperature increase on -1 Volt gate bias. 20
Figure 11. Albrecht's equation mobility vs. temperature. 23
Figure 12. Part A of Albrecht's equation mobility vs. temperature. 24
Figure 13. Part B of Albrecht's equation mobility vs. temperature. 24
Figure 14. Part C of Albrecht's equation mobility vs. temperature. 25
Figure 15. Albrecht's equation mobility vs. donor concentration. 25
Figure 16. Simulated Band Diagram. 29
Figure 17. I(A)-V curves comparing actual vs. simulated device. 30
Figure 18. 2D Model Room Temperature I(A)-V simulated and actual (RED). 31
Figure 19. 2D Model Lattice temperature plot for room temp simulation. Peak temperature 399º Kelvin. 31
Figure 20. 2D Model I(A)-V comparison at 400º and 500º Kelvin. 32
Figure 21. Comparison of I(A)-V curves for 2D and 3D model. 34
Figure 22. Comparison of I(A)-V curves for Block and Newton solver. 35
Figure 23. Comparison of global device temperature (K) for Block and Newton solvers. 35
Figure 24. Comparison of isothermal models for 2D and 3D. 36
Figure 25. Best match for 2D and 3D I(A)-V curves 37
Figure 26. Comparison of the thermal model and isothermal model I(A)-V curves. 38
Figure 27. 3D thermal model results. Red at 392º K to Blue at 300º K 39
Figure 28. 3D heating in channel under the gate. Red at 392º K 39
Figure 29. 3D electron concentration 40
Figure 30. 2D thermal image from middle of the device. 41
Figure 31. Temperature (K) profile of the device across the channel. 41
Figure 32. Comparison diamond and sapphire substrate I(A)-V curves 42
Figure 33. Comparison of global device Temperature (K). 43
Figure 34. Thermal image of diamond substrate HEMT. 44
Figure 35. Diamond substrate model channel temperature profile. 44
Figure 36. Electric field profile across channel 45
Figure 37. GaN on Diamond Proposed by SP3 From [13]. 49

THIS PAGE INTENTIONALLY LEFT BLANK

LIST OF TABLES

Table 1. Semiconductor Material Properties From [3]. 2
Table 2. Normalized figures of merit of various semiconductors From [4]. 3
Table 3. Structure parameters for Wurtzite nitrides From [12]. 11
Table 4. Substrate material properties..13
Table 5. Default Thermal Parameters for GaN From [21]...27

THIS PAGE INTENTIONALLY LEFT BLANK

ACKNOWLEDGMENTS

I would like to acknowledge the people who have helped me to work on this thesis. I would first like to thank Professor Todd Weatherford who provided me with the direction and focus to complete this thesis. The guidance given to me was invaluable in helping to create and run the simulations. The help in understanding the theory involved and your time to answer the questions I had is much appreciated. I would second like to thank Professor Parker who was the second reader of this thesis. I would like to thank the people at SP3 who work with developing diamond substrates for their input of ideas. Thank you also to those at Silvaco software company, especially Robin Jones that helped answer questions regarding the simulation software. I would last like to thank my wife and four children for their support during this process.

THIS PAGE INTENTIONALLY LEFT BLANK

EXECUTIVE SUMMARY

The currently deployed technology for the Department of Defense's high power radio frequency (RF) transmitters is the traveling wave tube. There are currently over 200 military systems that use the traveling wave tube technology [1]. The affordability issues, initial cost and maintenance, associated with these systems derive the need to examine lower cost alternative such as semiconductor technology. The current technology is Gallium Arsenide for solid state replacement for low power RF transmitters. This will not meet future needs of the DoD due to power and reliability limitations. The development of wide bandgap semiconductors such as Gallium Nitride has given a path for eventual use as a semiconductor replacement for traveling wave tubes.

The Gallium Nitride (GaN) material shows promise in high power applications due to its high electric field breakdown and induced channel charge. The heterojunction formation between GaN and Aluminum Galluim Nitride (AlGaN) induces a polarization charge. This charge creates a two-dimensional electron gas that has a high mobility allowing for high currents. There are many military applications for GaN such as radar, communications, and power. The semiconductor device examined in this work is the High Electron Mobility Transistor (HEMT). This device is specifically being considered by the Defense Advanced Research Projects Agency and Office of Naval Research for RF applications.

This research modeled the GaN device to investigate the effects of thermal heating. Device modeling allows for changes to be made in parameters easier and less expensive than having to manufacture the devices. The software used was provided by the Silvaco International Corporation. The software package used was the ATLAS^{TM} device simulator program. This program incorporated the use of BLAZE^{TM}, a heterojunction simulator, and GIGA^{TM}, a thermal modeling simulator. The basis for the modeling done was a GaN HEMT provided by UC Berkeley.

The Objectives of this research were to:

- Model HEMT band characteristics,
- Create a two dimensional (2D) model,
- Compare model results to actual device for various temperatures,
- Convert from 2D model to 3D model,
- Compare 2D to 3D results in order to verify model results,
- Change the substrate from Sapphire to Diamond.

The initial modeling was to establish an acceptable comparison in data between simulated and actual device characteristics. The modeling was initially done in 2D to allow for implementations of changes into the code. Then a 3D model was studied, which gave a more accurate prediction of the I-V characteristics over temperature.

The understanding of the effects of the thermal heating and heat dissipation in the device can lead to improvement in thermal management. The changes in the modeling of a sapphire substrate to a diamond substrate showed improved thermal management. The change lowered the operating temperature by 86º Kelvin for the device on diamond. The result was better current characteristics at the same biases. The results from this work show that for high power and reliability, GaN HEMTs on diamond substrates should result in an improved performance.

I. INTRODUCTION

A. BACKGROUND

Military systems have a wide range of applications that use Radio Frequency (RF) transmitters. These areas include radar systems, electronic warfare, satellite, and communication systems. To amplify microwaves and millimeter waves the current technology being used is the Traveling Wave Tube (TWT). There are over 200 military weapon systems that currently use TWT technology [1]. The size, reliability, and expense of the TWTs make them suitable for the option of replacing them with semiconductor technology. There is need for a high power, highly efficient, large bandwidth, and reliable semiconductor device. A possible solution is found in wide bandgap semiconductors such as Gallium Nitride (GaN).

The Traveling Wave Tube is the current technology used to produce high power RF Transmissions. They were invented during World War II by Rudolf Kompfner in a British lab and later refined by Bell Labs for communications. The device uses an electron gun to produce electron beam that moves through a helix to a collector. The microwave signal enters the tube at the end closest to the electron gun and is coupled to a helix coil. The energy from the electrons is transferred to the helix electromagnetic field. This creates an amplified microwave signal to the load at the helix output. The TWT can provide operations in the frequency range of 300 MHz to 50 GHz. They can operate over a wide bandwidth of up to one octave with a power gain of up to 60dB. They are capable of delivering continuous-wave power levels in the kilowatt range and pulsed power levels exceeding a megawatt. The Department of Defense (DoD) buys approximately two thirds of the TWTs manufactured. System failure studies show that TWTs are a major concern with reliability and that maintainability is the top cost driven issue at approximately 1.3 million dollars per ship in 2003 [2]. With the incumbent TWT technology, a semiconductor replacement must meet or exceed the operational characteristics at a lower cost.

Current semiconductor technology uses silicon or gallium arsenide (GaAs) for low frequency switching applications. Silicon devices are easily processed, cost effective,

however this technology does not allow for high frequency without the introduction of noise. GaAs has high electron mobility and a higher bandgap than silicon, allowing for higher frequency and lower noise operation. GaAs technology is currently used in cell phones and other communication systems, with limited applications in radar systems. The evolution of GaAs from MEtal-Semiconducting Field Effect Transistor (MESFET) devices in the late 80s to use in High Electron Mobility Transistor (HEMT) devices in the late 90s has allowed it to become the lead commercial amplifier technology in the cell phone industry. GaAs FET development was sponsored by the DoD in the 80s but only low power RF military applications could be supported with GaAs technology. GaAs currently lacks the high power and affordability to be a suitable replacement for the high power TWT applications. Table 1 shows a list of semiconductor material properties from Yoder [3].

	Si (----)	GaAs (AlGaAs/ InGaAs)	InP (InAlAs/ InGAs)	4H SiC (-----)	GaN (AlGaN/ GaN)
Bandgap (eV)	1.1	1.42	1.35	3.26	3.49
Electron mobility (cm^2/Vs)	1500	8500 (10000)	5400 (10000)	700	900 (>2000)
Saturated (peak) electron velocity ($x10^7$ cm/s)	1.0 (1.0)	1.0 (2.1)	1.0 (2.3)	2.0 (2.0)	1.5 (2.7)
2DEG sheet electron density (cm^{-2})	NA	$<4 \times 10^{12}$	$<4x10^{12}$	NA	$1\text{-}2x10^{13}$
Critical breakdown field (MV/cm)	0.3	0.4	0.5	2.0	3.3
Thermal conductivity (W/cm-K)	1.5	0.5	0.7	4.5 (3.3)[a]	>1.7
Relative dielectric constant (ε_r)	11.8	12.8	12.5	10	9.0

[a] thermal conductivity of SI-SiC

Table 1. Semiconductor Material Properties From [3].

Wide bandgap semiconductors, with bandgap greater then 2 eV, provide a feasible solution for high power and high frequency applications. The characteristics needed for a good semiconductor RF amplifier are high breakdown field strength, bandgap, saturated electron velocity, and mobility. The GaN and SiC parameters in Table

1 are beneficial for RF semiconductor amplifiers. Larger power handling capabilities are determined from the higher breakdown voltage. The higher thermal conductivity allows generated heat to be removed thus allowing for higher power operation for longer durations. The higher saturated electron velocity results in a higher operating frequency. A good comparison of the semiconductor characteristics is by using various figures of merit for scaling purposes. Table 2 is the comparison of semiconductors over four different figures of merit. Johnson's figure of merit (JFM) is the measure of a transistors power gain and frequency performance by using the product of the breakdown voltage (E_b) and saturation velocity (v_s). Keyes's figure of merit (KFM) provides for measuring thermal limitation to the switching behavior where ε is the dielectric constant, c is the speed of light, and κ is the thermal conductivity. Baliga's figure of merit (BFM) provides for minimizing the conduction losses in power devices where μ is the mobility and E_g is the bandgap. Baliga also developed a high frequency figure of merit (BHFM) which demonstrates a reduction in power losses at high frequencies. The figures of merits give a good quantitative comparison of the semiconductor material. This comparison shows that the desired performance traits of GaN make it the most viable option for high power high frequency RF amplifiers. Johnson's figure of merit is the most applicable for RF amplifiers.

	Si	GaAs	4H-SiC	GaN
JFM	1	11	410	790
KFM	1	0.45	5.1	1.8
BFM	1	28	290	910
BHFM	1	16	34	100

JFM : Johnson's figure of merit for high frequncy devices = $(E_b V_s / 2\pi)^2$

KFM : Keyes's figure of merit considering thermal limitation= $\kappa(c\ V_s / 4\pi\varepsilon)^{1/2}$

BFM : Baliga's figure of merit for power switching = $\varepsilon \mu E_g^3$

BHFM : Baliga's figure of merit for high frequency power switching = μE_b^2

Table 2. Normalized figures of merit of various semiconductors From [4].

The current maturity of the GaN FET technology does not allow it to be an immediate replacement for high power RF TWT. The current issues with GaN are in manufacturing and thermal management. This paper will look at improving thermal management by studying the effects of different substrates on the operation of GaN HEMTs. The improved thermal management will support better operation and improved reliability, possibly making GaN a suitable replacement for high power high frequency TWT.

B. RELATED RESEARCH

1. Summary of Previous Research

Previous research done at Naval Postgraduate School (NPS) examines the modeling of AlGaN/GaN HEMT devices using SILVACO ATLAS^{TM} software. The early research concentrated on developing an accurate model to study the operation of HEMT devices. These researchers were trying to develop routines for the sheet charge generated at the AlGaN/GaN interface. The software used for this model was updated to include and incorporate the work of Jon C. Freeman who looked at spontaneous and piezoelectric polarization fields [5]. With the modified software, improved models were developed by Salm [6] and Newham [7].

Salm's work transitioned from basic operation of the GaN HEMT device to examining the thermal effects. He also investigated the differences diamond and sapphire substrates had on the device operation. He was able to build simulations for a two dimensional (2D) and three dimensional (3D) model to examine the heating affects. Although he was unable to incorporate the piezoelectric function in the ATLAS^{TM} software for either model, he was still able to obtain accurate results. The thermal modeling observed an improvement in heating affects and operation when substituting sapphire substrate for diamond [6]. This led to the follow on research by Newham.

Newham's research created a improved model by comparing the actual device characteristics with simulations. He used a GaN on sapphire device from UC Berkeley that was developed by S. Tzeng [8]. He was able to measure current and voltage (I-V) characterization curves at various temperatures to see the effects of heating. He then compared the results to those modeled in the Silvaco software, which showed only a 13% difference between actual and simulated current. Although he was unable to incorporate

the piezoelectric function in the ATLAS™ software, he was able to use a sheet charge to model the piezoelectric effect of the HEMT channel. He incorporated the Albrecht model to optimize the simulated device characteristics to match the actual device. Once he accomplished matching device operating characteristics he was able to look at the effects of changing the simulation to use a diamond substrate. The results showed improved thermal and operating characteristics, which will lead to longer operational lifetime of the device [7].

The past improvement shown in device modeling at NPS has led to accurate predictions of how the device will operate over temperature. Incorporating the previous work will be helpful in continuing to develop a model studying reliability.

2. DARPA Wide Bandgap Semiconductor Technology Thrust I

Defense Advanced Research Projects Agency (DARPA) has set forth technical challenges to meet criteria for the use of GaN in military systems. The Wide Bandgap Semiconductor for RF Applications program is looking at GaN HEMTs as a replacement for TWTs. The program goals were to create a higher power, higher efficiency and higher bandwidth devices with improved thermal performance. Another goal is to achieve rapid insertion into DoD systems.

The challenges in producing a device capable of meeting these goals were set in DARPA's technical performance requirements. The device reliability must meet or exceed mean time to failure (MTTF) of greater than 10^6 hrs. The device must have a high operating frequency of greater than 40 GHz with a bandwidth of one decade. The resulting output must be able to produce high RF yields of over 50 percent. DARPA also set a technical challenge of thermal management of 1 kW/cm^2 [9]. These goals and technical challenges are to be met in a three phases.

Phase one of the program looked at the science and materials for wide bandgap semiconductors. The results from phase one showed a process improvement for creating high quality silicon carbide (SiC) substrates. Phase one also resulted in creating more uniform GaN epitaxy, by both molecular beam epitaxy (MBE) and metal organic chemical deposition (MOCVD). Phase one was twenty-four months then phase two examined device technologies. As of 2007 DARPA is currently in the middle of phase

two of the program which is thirty-six months long. Phase two will look at the best practices for device fabrication. The phase two program is investigating the degradation mechanisms, thermal management, reproducibility, and RF optimization. The end of phase two should result in X and Q band discrete device demos with the process for fabricating the devices. Phase three will look at electronic integration and circuit technologies. This phase is set to last twenty-four months with the results producing circuit demos of X and Q band Monolithic Microwave Integrated Circuits (MMIC).

DARPA also broke the program into three tracks for development of the GaN-based devices. Track one is looking at X-band transmit/receive modules for power and low-noise amplifiers. The lead for track one is Raytheon with an alliance with Cree. Track two is looking at Q-band high power amplifiers with Northrop Grumman Space technologies as its lead. Track three is looking at development of broadband high power amplifiers with Triquint semiconductors and academics partners. Part of Triquints research is looking into revolutionary steps to improve operation and thermal management. They have partnered with Group4Labs and SP3 to look at alternative substrates. Both companies are looking at different ways to fabricate diamond substrates for GaN devices. DARPA's program has so far shown promise that the GaN technology will be useful for defense programs. The evolutionary and revolutionary developments that the DARPA program has brought will result in enhanced capabilities and performance to GaN technology.

3. Navy Research

Navy research into GaN is under the 6.1 electronics program. The 6.1 program is a scientific inquiry into important areas for future navy applications. The Office of Naval Research (ONR) electronics science and technology program goals are based on developing and providing affordable high performance RF electronics to the war fighter. ONRs approach for wide bandgap devices cover research for GaN technology for solid state RF amplifier applications. They are looking at the advancement of GaN high frequency transistors through the Millimeter-Wave initiative for nitride electronics, process and device technologies, and new technologies. ONR is conducting research in process development by fundamental studies on GaN on SiC, basic material studies in

MBE growth, investigating deep level defects, and dielectrics for improved performance. ONR is also looking into the physics of failure for devices to find degradation mechanism of wide bandgap semiconductors [10].

C. OBJECTIVE

The purpose of this thesis is to look at the validity of modeling GaN HEMT device using ATLAS software. This will be a continuation of the previous research work conducted at Naval Postgraduate School. The goal is to create a device model simulation that accurately represents the actual device characteristics. This will be done by measuring and comparing actual device parameters of current versus voltage curves to those produced by the simulation software. Once a satisfactory 2D model is developed the modeling will be altered to create 3D model. The differences in modeling between the 2D and 3D simulations will be examined. The comparison will allow for determination of the better representation of the actual device to use to study the thermal effects. While studying the thermal effects of the device the substrate will be changed. The substrate change will show how operating characteristics may vary by improving the ability to remove heat from the channel.

THIS PAGE INTENTIONALLY LEFT BLANK

II. HIGH ELECTRON MOBILITY TRANSISTORS (HEMT)

A. HEMT FUNDAMENTALS

1. AlGaN/GaN HEMT

The AlGaN/GaN hetero-structure is used to take advantage of the two dimensional electron gas (2DEG). The interface of the AlGaN/GaN materials creates piezoelectric and spontaneous polarization effects using an undoped hetero-interface. The result is a high density electron gas with a high mobility. This channel of high mobility electrons contributes to naming the device the High Electron Mobility Transistor (HEMT). This device has also has been referred to as the modulation doped field effect transistor (MODFET), selectively doped hetero-field-effect transistor (SDHT), and the two dimensional electron gas field-effect transistor (TEGFET), but HEMT has become the most common name for the device. The common structure for a typical HEMT device is shown in Figure 1 [11], showing the layers of the device and the location of the 2-DEG. This section of the thesis will go over basic operation of the HEMT device.

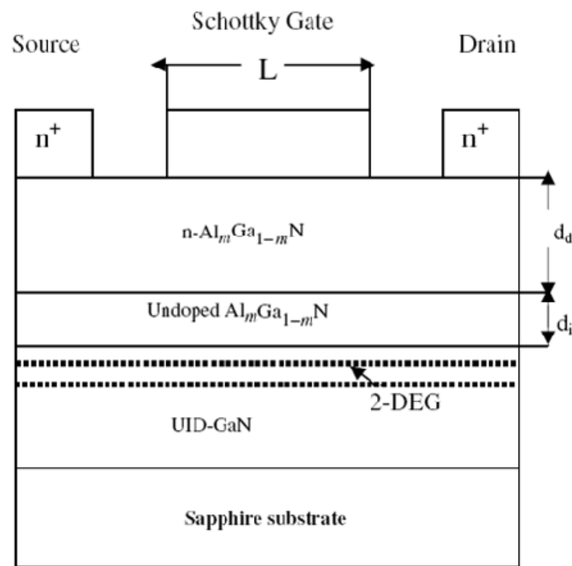

Figure 1. Typical AlGaN/GaN HEMT From [11].

To get an understanding of the HEMT operation, the material properties of GaN, AlGaN, AlN and the substrate material require investigation and description for device

modeling. The typical GaN structure forms a crystalline Wurtzite lattice, but under certain growth conditions can form a zinc-blend structure. The work in this thesis will look at and use the Wurtzite lattice structure shown in Figure 2. For the typical AlGaN/GaN HEMT the device will have a Gallium face to the thin-film AlGaN. This is dependent on growth conditions and material it is grown on. With the sapphire substrate it can be directly grown on and results in a Gallium face with the Nitride face bonding to the sapphire. The material issues for growing GaN have to look at lattice matching and use of a transition material to the substrate. Typical methods for growing GaN are using MBE or MOCVD.

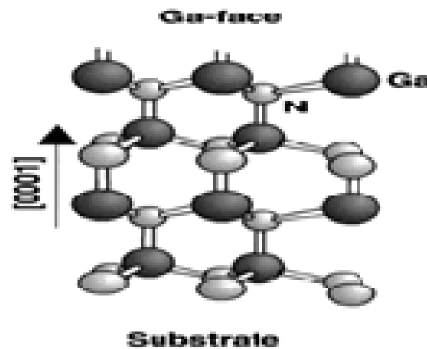

Figure 2. Crystal structure of Wurtzite GaN From [7].

GaN is a direct bandgap material which has led its application in lasers and LEDs. The energy gap in Wurtzite GaN is approximately 3.5 eV [12] which makes it an ideal material for high voltage applications. Reported in the *Applied Physics Review* [12] is the temperature dependence of the GaN energy gap varying 72 meV over a range of 0 to 300º Kelvin. The other important properties for the GaN materials that need to be looked at are the effective mass for electron and holes, valance band deformation potentials, elastic constraints, piezoelectric coefficients, and the calculations for spontaneous polarization. The characteristics are summed up in Table 3 from Vargaftman et al. [12] which are based on averages and best value numbers. These values are similar to those used in the calculations by Freeman. These material properties are used to build the determination of the charge sheet properties for the 2DEG.

Parameters	GaN	AlN
a_{lc} (Å) at $T = 300$ K	3.189	3.112
c_{lc} (Å) at $T = 300$ K	5.185	4.982
E_g (eV)	3.507	6.23
α (meV/K)	0.909	1.799
β (K)	830	1462
Δ_{cr} (eV)	0.019	−0.164
Δ_{so} (eV)	0.014	0.019
$m_e^{\parallel}$	0.20	0.28
$m_e^{\perp}$	0.20	0.32
A_1	−6.56	−3.95
A_2	−0.91	−0.27
A_3	5.65	3.68
A_4	−2.83	−1.84
A_5	−3.13	−1.95
A_6	−4.86	−2.91
E_P (eV)	14.0	14.5
F	0	0
VBO (eV)	−2.64	−3.44
a_1 (eV)	−6.5	−9.0
a_2 (eV)	−11.8	−9.0
D_1 (eV)	−3.0	−3.0
D_2 (eV)	3.6	3.6
D_3 (eV)	8.82	9.6
D_4 (eV)	−4.41	−4.8
D_5 (eV)	−4.0	−4.0
D_6 (eV)	−5.1	−5.1
c_{11} (GPa)	390	396
c_{12} (GPa)	145	137
c_{13} (GPa)	106	108
c_{33} (GPa)	398	373
c_{44} (GPa)	105	116
e_{13} (C/m^2)	−0.35	−0.50
e_{33} (C/m^2)	1.27	1.79
P_{sp} (C/m^2)	−0.029	−0.081

Table 3. Structure parameters for Wurtzite nitrides From [12].

The material properties for AlN in Table 3 are from the *Applied Physics Review* [12]. This material is typically used as a buffer layer between substrates and GaN layer. This material is not typically used in devices and is only a concern if used as a buffer layer because this layer will have impact on the thin film strain. This material is also used in the growth process of most HEMT devices.

The other main material in the heterojunction is AlGaN which is a ternary alloy. The energy gap for the material will be based on the composition of the alloy. The alloy composition is controlled by $Al_xGa_{1-x}N$ in which x is the percentage of Aluminum concentration. This becomes an important factor in the operation of the HEMT device. The concentration affects the amount of band bending that occurs in the conduction band and therefore affects the operation of the device. Also the material thickness will have an affect on the operation by changing the stress in the thin film. These effects will be discussed later.

The Schottky Gate is the common metal gate contact for III-V FETs. The material chosen for the Schottky gate varies with transistors designs. The gate metal is Ti, Al, Ni, or Au or an alloy composed of two or more of these materials. The alloy composition and the choice of deposition method of the alloy will have an effect on the Fermi level in the material. Research into gate characteristics has shown that there are various physical properties, such as shape of the gate, placement and the use of buffer layers. The main properties encountered are involving the gate leakage and capacitance and how they effect the operation of the device. The basic Schottky gate will be used for the modeling in this thesis.

The last material component is the substrate on which the device sits and provides mechanical support. The substrate is the material in which the devices are fabricated. For GaN technology the typical substrates are sapphire or silicon carbide (SiC). This thesis looks into the use of a polycrystalline diamond substrate. The important material properties to study are thermal conductivity, thermal expansion, lattice size and structure. These properties, listed in Table 4, were gathered from various sources including physics journals and data obtained from SP3 corporation [5] [11] [13] [18].

Material	Sapphire	SiC (6H)	Poly Diamond
a Lattice contant (Å)	4.75	3.08	N/A
c lattice constant (Å)	12.99	15.12	N/A
Thermal conductivity W/m-K	25-40	350	1200
CTE µm/m -°C	5	10.3	1.5-1.8

Table 4. Substrate material properties.

The polycrystalline diamond is manufactured by SP3 and is grown on a silicon wafer. The lattice data is not listed because a thin layer of silicon will remain in between the diamond and the GaN layer. This layer will have an effect on the overall strain between the GaN/AlGaN heterostructure layers. For this thesis this layer of silicon will be ignored.

The material properties are important in determining the strain in GaN films. The factors affecting the strain are examined by Freeman [5] and Kisielowski et al. [14] [15], who identified the origins and effects of strain on GaN films. The Lattice mismatch and the effect of the thermal expansion coefficients in the growth process are the major factors that affect the strain. The growth process is typical done by MBE and MOCVD with temperatures in the range of 500 to 1300 K. The higher the temperature the more of an affect the thermal coefficient of expansion will have. The bending due to thermal expansion is shown in Figure 3 from Freeman [5] and uses Equation 1 for determining strain. The bending is a benefit in adding strain in the thin film to increase the piezoelectric and sheet charge, which will be explained in a later section.

$$\sigma_{\mathrm{j}}(y) = E\left[\sum_{i=1}^{N}\left(\frac{t_i \in_{ij}}{t} + \frac{t_i \kappa_i}{2R}\right) + \frac{y - \frac{t_j}{2}}{2R}\right] \quad (1)$$

Where: R is the radius of curvature (m), E is the elastic moduli (Gpa), $\in$ is the layer strain (dynes/cm^2), t is the thickness (m), κ=+1 for i<j, κ=0 for i=j, κ=-1 for i>j, y is distance from the bottom of layer (m).

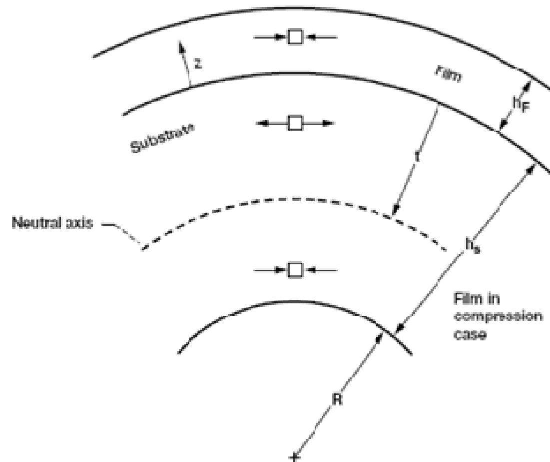

Figure 3. Bending and strain due to different thermal expansion coefficients From [5].

The negative effects of induced strain can also affect the device. The introduction of lattice defects and delaminating between layers has been noted to occur due to strain. The bending or bowing can be seen at the wafer level and makes it difficult to process using lithography. These defects introduce reliability issues and introduce electron traps reduce performance and life-time. The physical properties such as bandgap and chemical composition are altered by strain [15]. The strain can be controlled by introduction of buffer layers and film thickness. This thesis will look at the layers set up by the UC Berkeley device for the development of the sheet charge characteristics.

2. Two Dimensional Electron Gas (2DEG)

In bulk semiconductors the electrons move freely in all three dimensions allowing interaction with the materials atoms. This interaction of electrons is typically collision with atoms that cause scattering and the electrons lose some kinetic energy. This results in transfer of energy to the lattice producing phonons and thus heating. The two dimensional electron gas (2DEG) is the creation of a plane of electrons to transport in only two dimensions. This is done by the formation of a quantum well below the Fermi energy in the conduction band. Figure 4 shows the band diagram for the AlGaN/GaN heterojunction based on depth through device. This well can be varied by changing the material properties such as thickness and Al concentration.

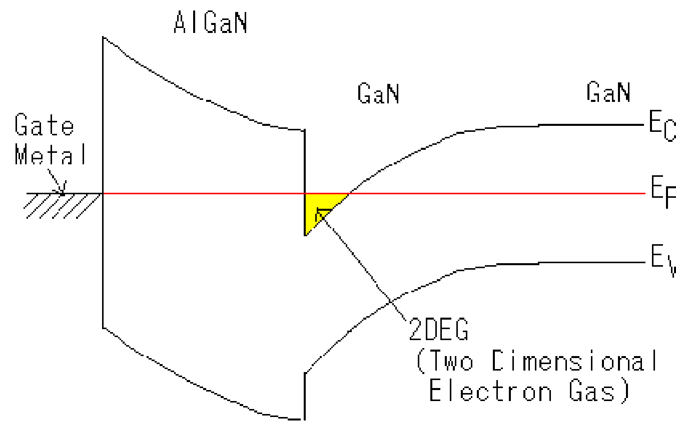

Figure 4. Band Diagram of AlGaN/GaN Heterojunction From [5].

The work by Maeda et al. [15] shows the calculations for determining the charge density for the 2DEG. Figure 5 shows the results of these calculations using a lattice relaxation ratio of the barrier layer. The un-relaxed calculations showed a higher density with this being the more strained layer. This is shown again in the work of Mastro [17] who studied the effect of non-uniform strain. This presents the effect of AlGaN layer relaxation as a factor of layer thickness and composition and gate width dependence. Both lead to the ability to determine charge density of the 2DEG. The next part looks at polarization effects of the heterojunction that have an effect on the carrier concentration in the 2DEG.

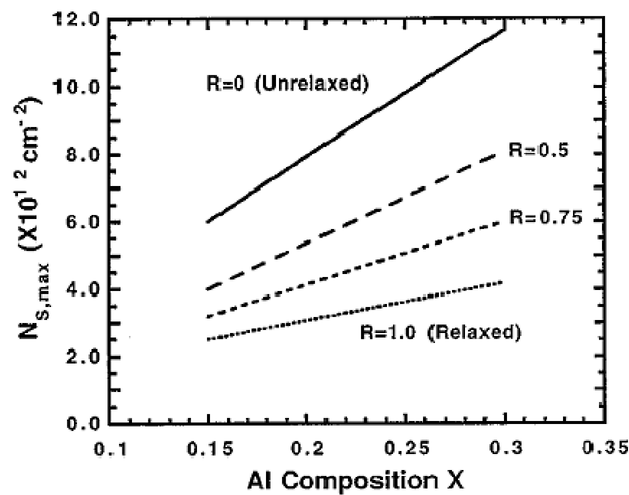

Figure 5. Sheet charge density based as a function of Al composition From [15].

3. Piezoelectric and Spontaneous Polarization

This section investigates the effects that create the 2DEG, piezoelectric and spontaneous polarization. The sheet charge is a result of the total polarization from both sources. This is shown by Freeman [5], Bernardini [18], and Ambacher[19]; each develop total polarization as the sum of the two sources of polarization. The spontaneous polarization is the charge that is developed by the structure of the material. Piezoelectric polarization is the charge that is developed by strains in the material. The GaN Wurtzite crystal structure will be looked at for determining the polarization effects in the structure.

The GaN layer is the basis for the development of the total sheet charge. Previous research looked at the GaN layer as being unstrained and therefore producing no piezoelectric charge [5][18][19]. The AlGaN layer is considered under stress due to a lattice mismatch which is dependent on Al composition. The AlGaN layer thickness also affects the overall strain. The defect densities are also another factor to calculate for strain. For this thesis, defect densities are not studied. The piezoelectric effect is assumed to be linear based on composition. Both Ambacher and Freemen presented Poisson's and Schodinger's equations to solve for piezoelectric polarization. The equations will not be used, but the final values will be for the calculated sheet charge.

The spontaneous polarization is mainly effected by bond structure and length with anions and cations. The spontaneous polarization is derived from Ambacher's work shown in Figure 6 [18]. This will allow us to determine the polarization charge for both GaN and AlGaN based on composition. The direction of polarity is also important for resolving the total polarization. This thesis only examines GaN-faced Wurtzite crystal structures.

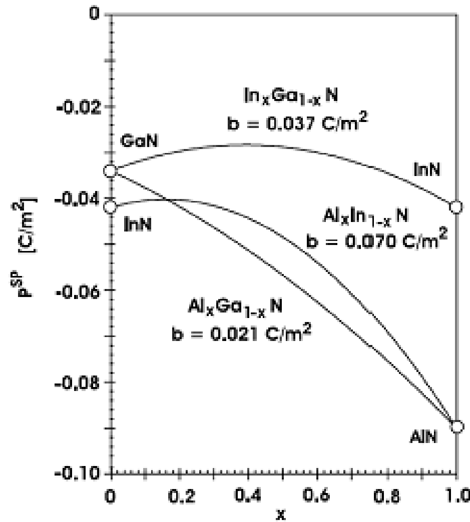

Figure 6. Spontaneous polarization for Wurtzite crystal From [18].

4. Thermal Effects

The effects of thermal heating on mobility in the GaN HEMT were examined by Albrecht [20] who modeled them in an equation. The calculations were done for low field mobility using a Monte Carlo simulation. The results from the Albrecht model are shown in Figure 7 and will be discussed in the modeling section. Another thermal effect is joule self-heating that produces localized hot spots in the channel. Self-heating is analyzed in the modeling.

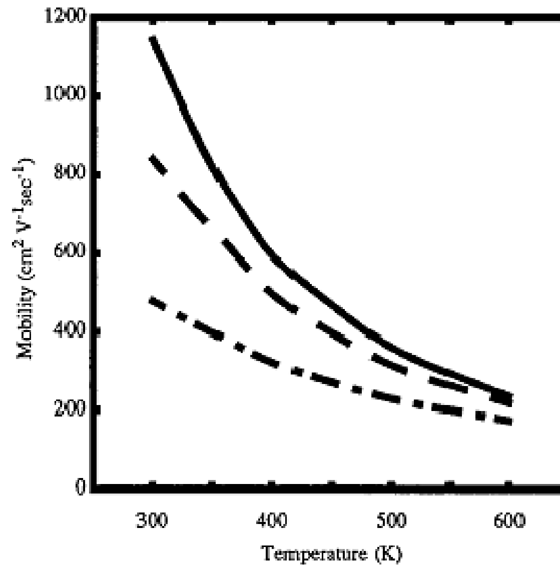

Figure 7. Low field electron mobility for GaN donor concentrations 10^{16}/cm^3 (solid) 10^{17}/cm^3 (dashed) 10^{18}/cm^3 (dashed dotted) From [20].

B. UC BERKELEY DEVICE

The actual physical device measured for this research was from the University of California, Berkeley and was used in the work by Tzeng [8]. The GaN HEMT device was grown by metal-organic chemical vapor deposition on a sapphire substrate. The device consisted of a GaN buffer layer, 1.5 micron unintentionally doped GaN layer, and approximately a 25 nanometer unintentionally doped AlGaN layer. The sample device Naval Postgraduate School received had an AlGaN thickness of 26.7 nanometers and a composition of 28%. The ohmic contacts for the source and drain were Ti/Al/Ni/Au alloy deposited be e-beam evaporation. Measured contact resistance was approximately 5e-6 Ω-cm^2. The Schottky Gate used was a Ni/Au alloy deposited by e-beam evaporation. The gate lengths provided were 2, 3.5, and 5 microns and widths of 50, 100 and 150 microns. The device is shown in Figure 8 using a scanning electron microscope [8].

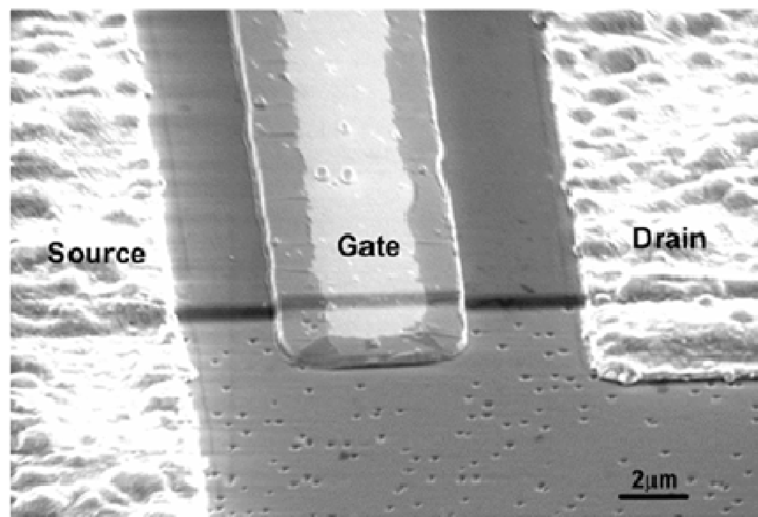

Figure 8. SEM image of GaN HEMT From [8].

1. Testing the UC Berkeley Device

The Hall Effect measurements results are from the work done by Tzeng [8]. The sheet charge from this measurement was 9.24e12 cm^{-2} and the mobility of 1304 cm^2/V-sec. The sheet charge results are in agreement with the data from Maeda and Ambacher discussed earlier.

The DC characteristics were measured by Newham [7] at the Naval Postgraduate School. The testing was done on the Micromanipulator™ using the UTMOST™ program with a HP 4142B DC source. The measurements were done with a hot chuck and runs were done at room temperature 300º K, 400º K, 500º K, and 600º K. The results from Newham's [7] testing on the physical device will be used in this thesis and are discussed in the next section.

2. Results from UC Berkeley Device

The Berkeley device tested at Naval Postgraduate School demonstrates the effects of thermal self-heating where drain current drops with increase drain voltage. The device was measured at room temperature and the data was transferred into Silvaco TONYPLOT™ for evaluation. The DC I-V characteristic curves shown in Figure 9 are for gate bias of -1, -2, -3, -4, and -5 volts from top to bottom. This will be used later when comparing the modeled device to the actual device characteristics.

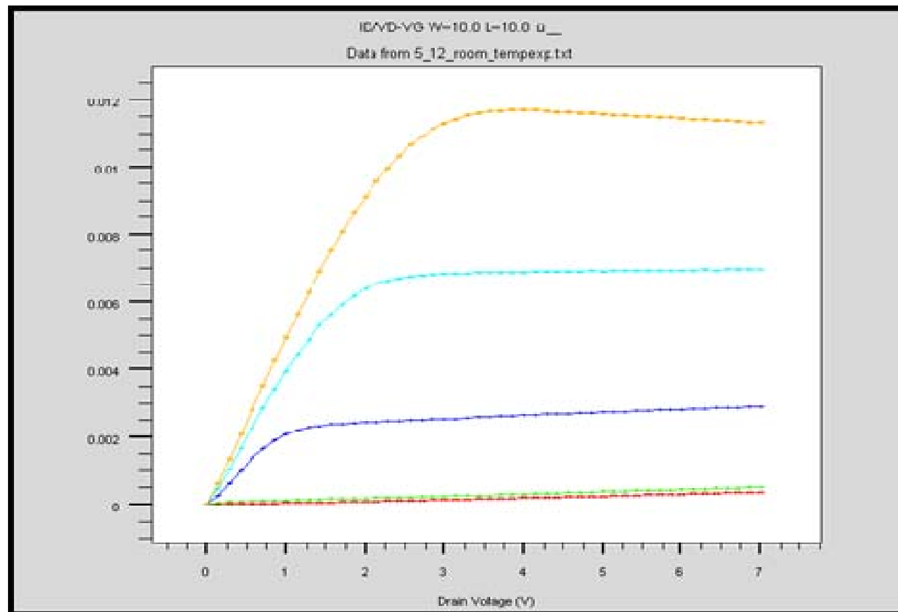

Figure 9. Room temperature (300º K) I(A)-V curves for UC Berkeley device.

The hot chuck heating affects can be seen by looking at the I-V curves over the spread of temperatures. Figure 10 shows a gate bias of -1 volt over a temperature range of 300º K to 600º K. This shows that as temperature increases the peak current is reduced. The self heating affects are seen in the top curve, which are at room temperature.

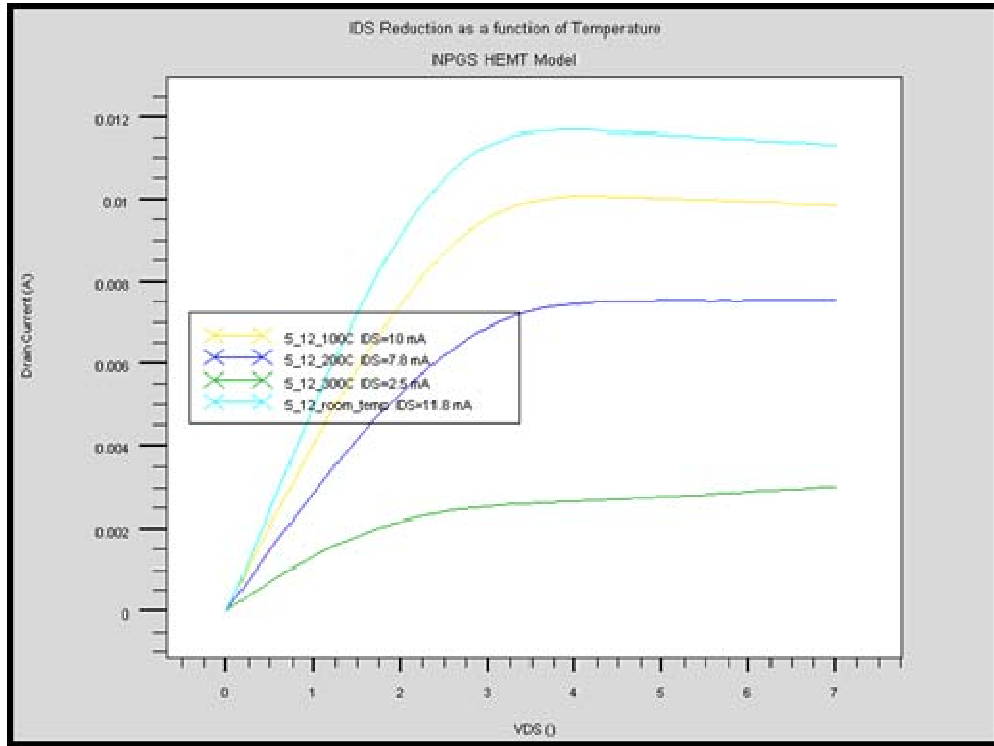

Figure 10. Current effects of temperature increase on -1 Volt gate bias.

The results of the measured physical device give an idea of expected values for the modeled device. The next section will go over the development of the model used in this thesis.

III. HEMT MODELING

A. MODELING HEMT ON SAPPHIRE

1. Model Design

The modeling was done using the Silvaco ATLAS^{TM} device simulation software. The goal of the modeling was to produce a model that can validate the characteristics seen by the actual device. The initial model was taken from Newham's [7] work. The model was set up with dimensions to match the physical device that was measured, using a 100 micron width and a 2 micron gate length. This section will discuses the changes made to Newham's model and the incorporation of ATLAS^{TM} model statements. The changes made were from studying the work looked at in Chapter II of this thesis and the Silvaco Atlas Manual from 2007 [21]. The present ATLAS^{TM} program incorporates modifications specifically for the simulation of heterojunction devices.

The first investigation was to the meshing of the input file for Deckbuild^{TM}. The three dimensional modeling needed reduced meshing points and spacing, to satisfy the nodal limit is 200,000. The first run of adding z-axis meshing was to extend the two dimensional model into a 10 micron device. This was successful in producing a three dimensional image however, the voltage sweeps required 5 or more hours to simulate. The mesh points needed to be reduced in order to extend the model to 100 micron gate width in order to match the physical device. With input from Robin J. Jones of Silvaco International the mesh points were reduced and the spacing increased. Reducing nodes can possibly reduce the accuracy of the simulation. The first attempt at running the new 3D model showed 556,800 nodes, so the points had to be reduced below 200,000. The x and y axis points were reduced first and no degradation to simulation accuracy was observed. The z-axis spacing was doubled and that produced 198,650 nodes which satisfied the limit. This still resulted in run time errors when running the file. The z-axis mesh spacing was doubled again resulting in a reduction to 99,325 nodes. This mesh was successful as a 3D mesh and was incorporated into the 3D model.

The next part of the research was to determine the mobility equations to use. In Newham's[7] work, he had used Albrecht's equation for modeling GaN devices. The

equation is already set up in the ATLAS™ software program based on Albrecht's paper on electron transport characteristics of GaN [20]. Albrecht had used a Monte Carlo simulation to develop his equation listed below, Equation (2).

$$\frac{1}{\mu} = a\left(\frac{N_I}{10^{17}\,cm^{-3}}\right)\ln\left(1+\beta_{CW}^2\right)\left(\frac{T}{300K}\right)^{-1.5} + b\left(\frac{T}{300K}\right)^{1.5} + \frac{c}{\exp\left(\Theta/T\right)-1} \tag{2}$$

Where:

T is the temprature in Kelvin

N_I is the ionized donor concentration (cm^{-3})

$$\beta_{CW}^2 = 3.00\left(\frac{T}{300K}\right)^2\left(\frac{N_I}{10^{17}\,cm^{-3}}\right)^{-2/3}$$

Albrecht had found that this was a viable equation to use from a range of 300 to 600º K and applied to electric field ranges from 0 to 500 kV/cm. This thesis implement Albrecht's equation for modeling the mobility. Albrecht had assigned constants to the values a, b, and c which are listed below. Newham [7] had altered the values of the constants to fit his model to measurements. The work for the 2D model encompasses using Albrecht's values of the constants as unchanged. The constant values are listed, where Θ is the photon temperature incorporating the phonon heating effects.

$$\Theta = \frac{\hbar\omega_{LO}}{k_B} = 1065K$$

$$a = 2.61\times10^{-4}\ V\text{-}s\text{-}cm^{-2}$$

$$b = 2.90\times10^{-4}\ V\text{-}s\text{-}cm^{-2}$$

$$c = 1.70\times10^{-2}\ V\text{-}s\text{-}cm^{-2}$$

For this thesis, MATLAB™ was used to determine the effects of temperature on mobility. Albrecht's equation was programmed into MATLAB™ code which is attached as Appendix A. This code was written to look at the effects of changes in temperature on each part of the equation. Albrecht's equation was broken down into three parts based on the constants. Figure 11 shows the effects of mobility versus temperature for the sum of parts A, B and C. Figure 12 shows part A of the equation, ionized impurity scattering, which is then plotted as mobility versus temperature. Part A of the equation is not only affected by temperature, but also by the ionized donor concentration. For this test of mobility versus temperature, ionized donor concentration was held constant at a value of

1e16/cm^3. Figure 13 shows part B of the equation, acoustic phonon limited mobility, plotted as mobility versus temperature. Figure 14 shows part C of the equation, longitudinal optical phonon limited mobility, plotted as mobility versus temperature. The effect of changing the ionized donor concentration on mobility was looked at and is shown in Figure 15. For this model ionized donor concentration will not be used because all material will be assumed to be undoped. This is a change from Newham's model which had doping levels.

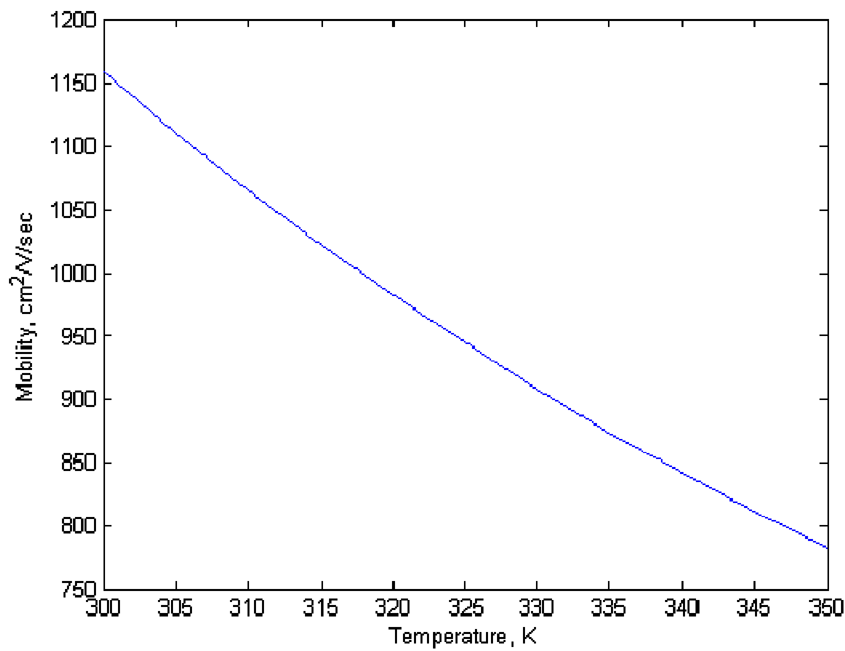

Figure 11. Albrecht's equation mobility vs. temperature.

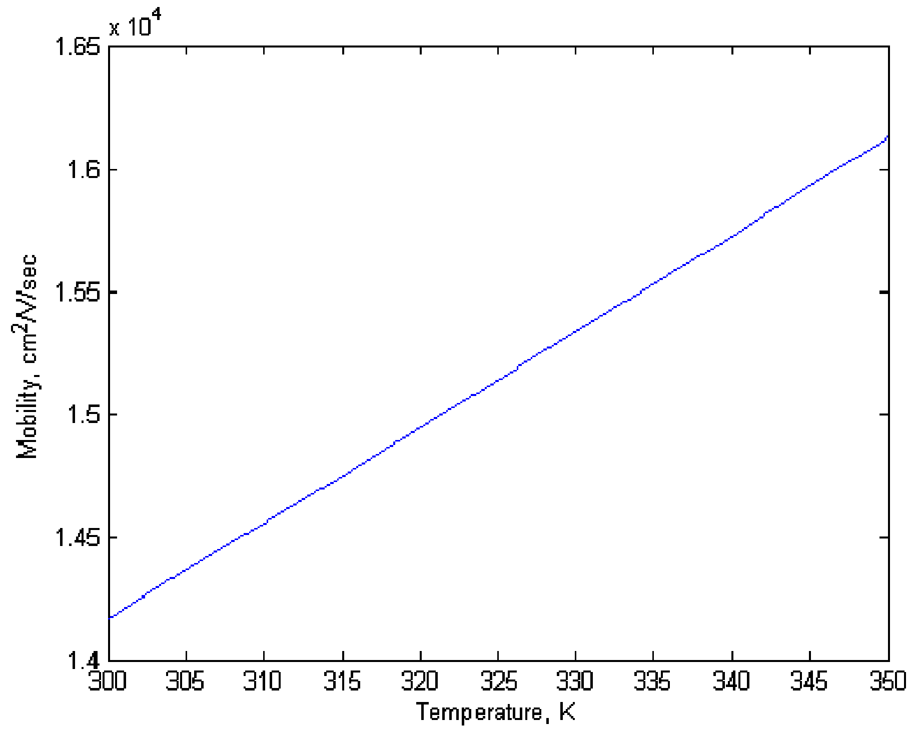

Figure 12. Part A of Albrecht's equation mobility vs. temperature.

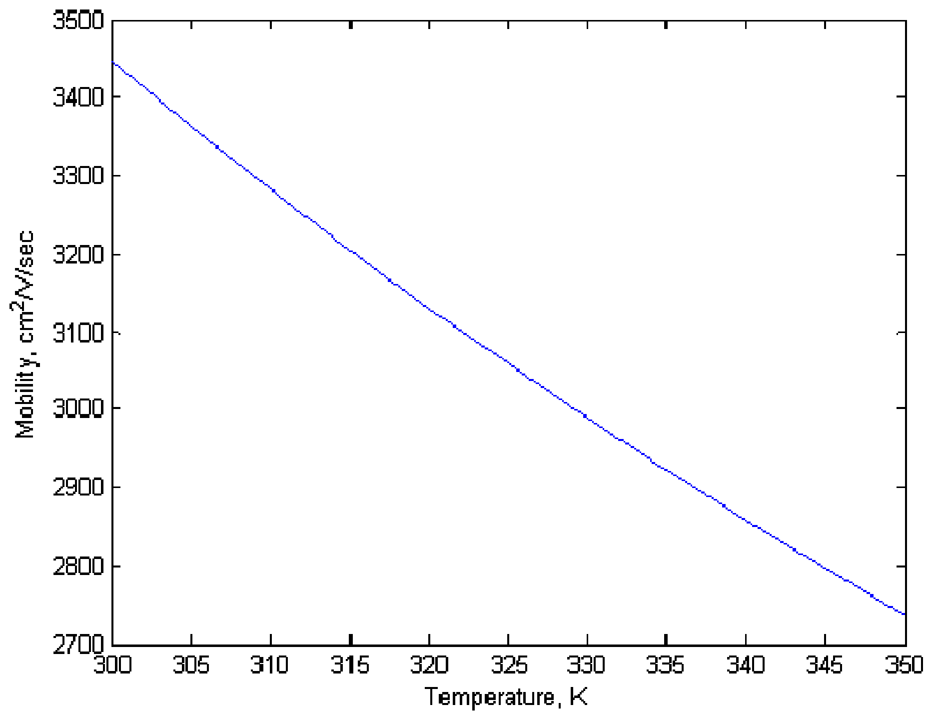

Figure 13. Part B of Albrecht's equation mobility vs. temperature.

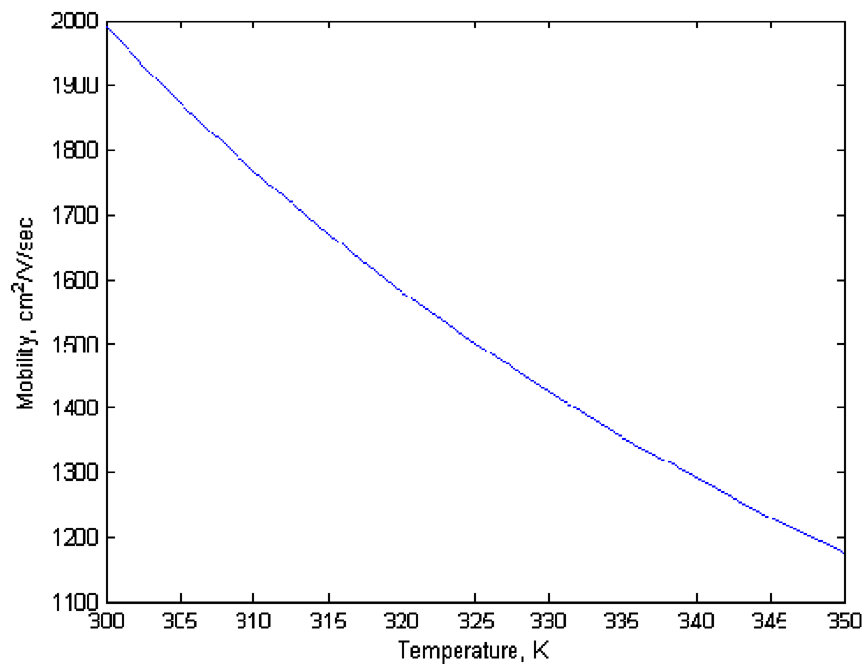

Figure 14. Part C of Albrecht's equation mobility vs. temperature.

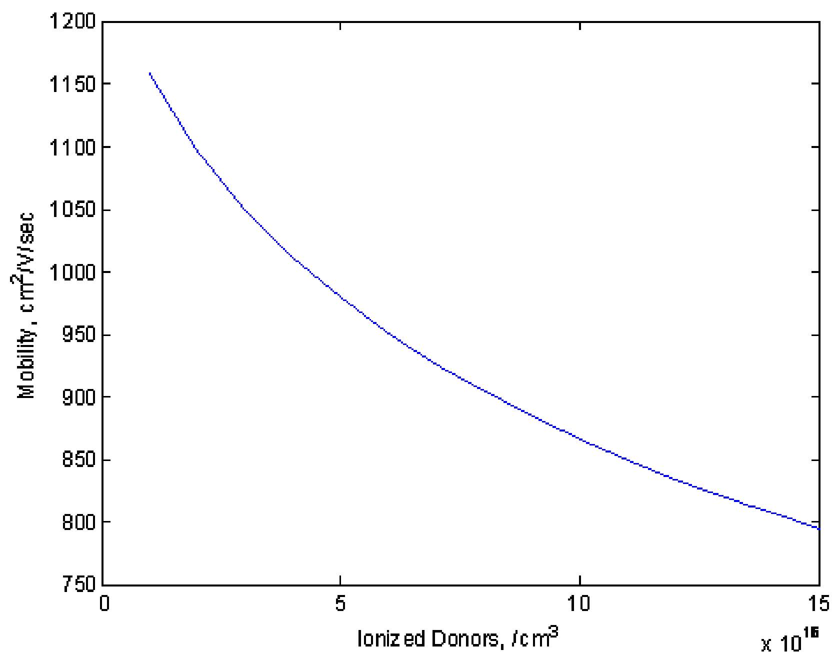

Figure 15. Albrecht's equation mobility vs. donor concentration.

The vertical axis for the plots in Figures 11-15 is defined as mobility in units of cm^2/V-sec. The results of this show that part A had the most effect on mobility, but parts B and C together are more effected by changes in temperature. The overall combination of the three parts together show that as temperature increases mobility decreases. This is important when we consider the self-heating that occurs in the GaN HEMT. The self-heating effects can be seen on the I-V measurements in the section on testing the UC Berkeley Device. The top curve on Figure 9 has a negative slope for current which reflects the lower mobility caused by self-heating. There were no temperature readings taken on the UC Berkeley device while it was under operation. The self-heating effects are looked at in the paper by McAlister [22]. McAlister showed that in GaN HEMT self heating can exceed increases of 100º Kelvin. For McAlister's simulations he also used Silvaco's ATLAS^{TM} software for modeling the GaN HEMT. The two dimensional electron gas was simulated by using a doping level of 5e19 cm^{-3} in a 2 nm channel in McAlister's model. This was attempted to be incorporated in this thesis model for simulating the self-heating effects.

The result of attempting this method of simulation of the self-heating effects was found to be unsuccessful. The doping levels at that concentration proved to create a short from drain to source and no self-heating was observed. Attempts to lower the concentration to a value that would produce the heating effects without creating a short proved difficult. Having the doping at a level of $1e15/cm^2$, which was the value Newham used, proved to have no effect on heating or operation of the device. A doping level of $1e17/cm^2$ showed to have heating of the device but changed the operating characteristics which resulted in a high current. Many manipulations of the Schottky work function were done with the change in donor concentration however; the desired effects were not able to be produced. This method for incorporating the self-heating effects was not successful.

The next part of developing this model was incorporating ATLAS^{TM} functions that had been developed for GaN modeling since Newham's thesis. The use of the new polarization function was attempted to be able to model the effects of spontaneous and piezoelectric polarization. These attempts were unsuccessful, which may be due to understanding how to implement this function. Therefore a sheet charge was implemented using the INTERFACE statement. The sheet charge for this model will

match the results from Tzeng's [8] testing of the Berkeley Device. The value of 9.3e12/cm^2 was used in this model. This value is also concurrent with those found in the papers by Freeman [5] and Ambacher [18].

For thermal conductivity and heat capacity for the material, it was determined that using the default equations were sufficient. Newham had used the standard model TCON.POLYN for the thermal conductivity of the GaN, AlGaN, and sapphire. This was not changed for the sapphire, but the GaN and AlGaN were set to use the default equations given below. In Equation (3) C is the heat capacitance per unit volume, ρ is the density of the material, Θ is the phonon temperature, and T is the temperature of the lattice. In Equation (4) κ is the thermal conductivity and δ is a kinetic coefficient for temperature dependence. Shown in Table 5 are the default parameters for GaN [21].

$$C_L(T) = C_L(300K)\frac{20-(\Theta_D/T)^2}{20-(\Theta_D/300K)^2}\rho_L \tag{3}$$

$$\kappa_L(T) = \kappa_L(300K)\left(\frac{T}{300K}\right)^{\delta_K} \tag{4}$$

•

Parameter Unit	κ_L (W/Kcm)	C_L (Ws/gK)	ρ_L (g/cm^3)	Θ_D (K)	δ_κ
GaN	1.30	0.49	6.15	600	-0.28
AlN	2.85	0.6	3.23	1150	-1.64
InN	0.45	0.32	6.81	660	0.0

Table 5. Default Thermal Parameters for GaN From [21].

The thermal properties also have an effect on the heating of the device. The self heating effects by Freeman focusing on channel temperature modeling was examined [23]. The work by Freeman showed an increase in peak channel temperature of 180º Kelvin for a similar power device for 20 volts applied. The only way found to incorporate this into the 2D model for this thesis was to change the thermal properties for the GaN layers. This was done by changing the TC.A parameter in the material statement. This resulted in a matching the temperature effect as seen by Freeman.

The next modification was to incorporate a step junction for the GaN and AlGaN heterojunction. This was done by following the Silvaco ATLAS^{TM} user's manual [21] on creating a step junction, an abrupt heterojunction between two materials. This was done by removing the Y.MIN designation in the region statement for the AlGaN and the Y.MAX designation from the GaN region statement. This allows for the simulation of the abrupt heterojunction parallel to the x-axis for semiconductor regions of different bandgap. This concluded the changes that were implemented by Silvaco for GaN devices.

The 2D model was run with the incorporated changes of returning Albrecht's constants to the given default values. This resulted in a current of approximately four times what was seen in the results from testing the UC Berkeley device. This was compensated for by adding contact resistance at the source and drain. The value chosen for the resistance was 5e-6 Ω-cm^2 which is from Tzeng's [8] measurements of the actual device. The results of adding this contact resistance brought the current to a level that was consistent with those seen in the I-V characteristics measured in the actual device. The bandgap curves matched the theoretical expectations for a GaN device and the result is shown in Figure 16. The modeling results will be discussed further in the next section.

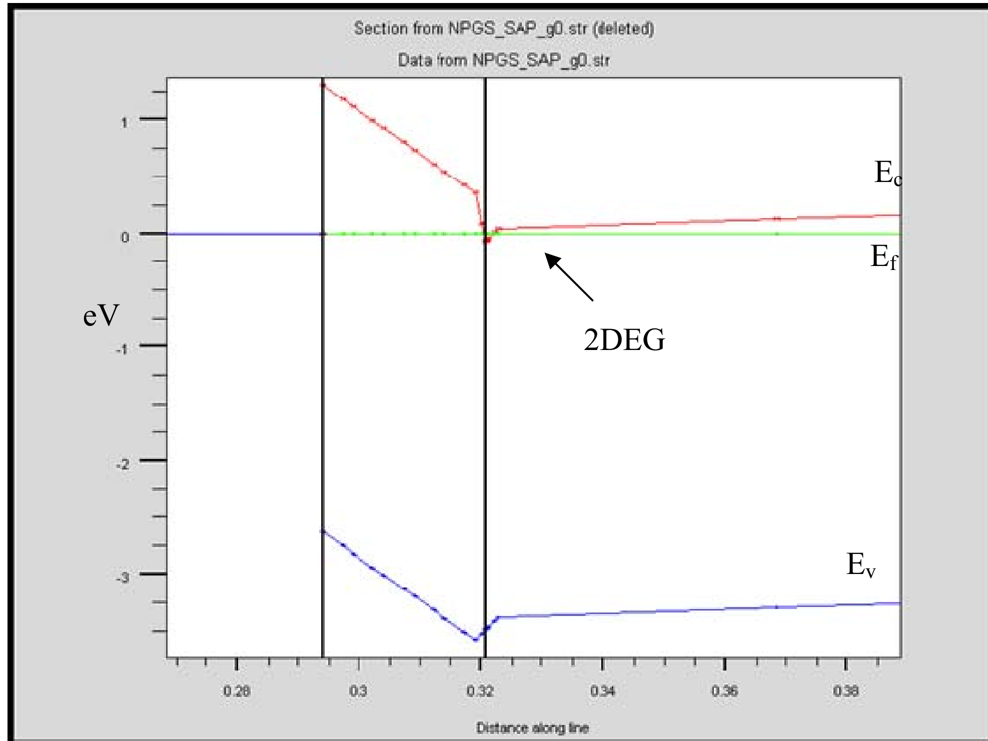

Figure 16. Simulated Band Diagram.

2. Comparison to Results from UC Berkeley Device

The model was initially run in two dimensions with an auto mesh width set at one hundred microns. Running the model in two dimensions first allowed it to run quicker in order to verify proper results. The initial runs did not incorporate the self heating affects with the changes in thermal conductivity. The peak temperature in the channel was only increased by 4º K, which does not match the results from the actual device. The simulation was run at room temperature, 300º Kelvin, and at 400º Kelvin. The results were compared to the physical device measurement as shown in Figure 17. The plot was done with an overlay in TONYPLOT™. In order to do the overlay the actual measured value data line called "VD()" had to be changed to "Drain Voltage". The Green line is the simulated I-V for the room temperature device. The Red line is the device measurements at room temperature. The Blue line the simulated run for the device at 400º Kelvin. This shows that the average temperature increase for the actual device is approximately 100º Kelvin for this data run. The rest of the simulation runs incorporated changing the thermal properties to include the self heating affects.

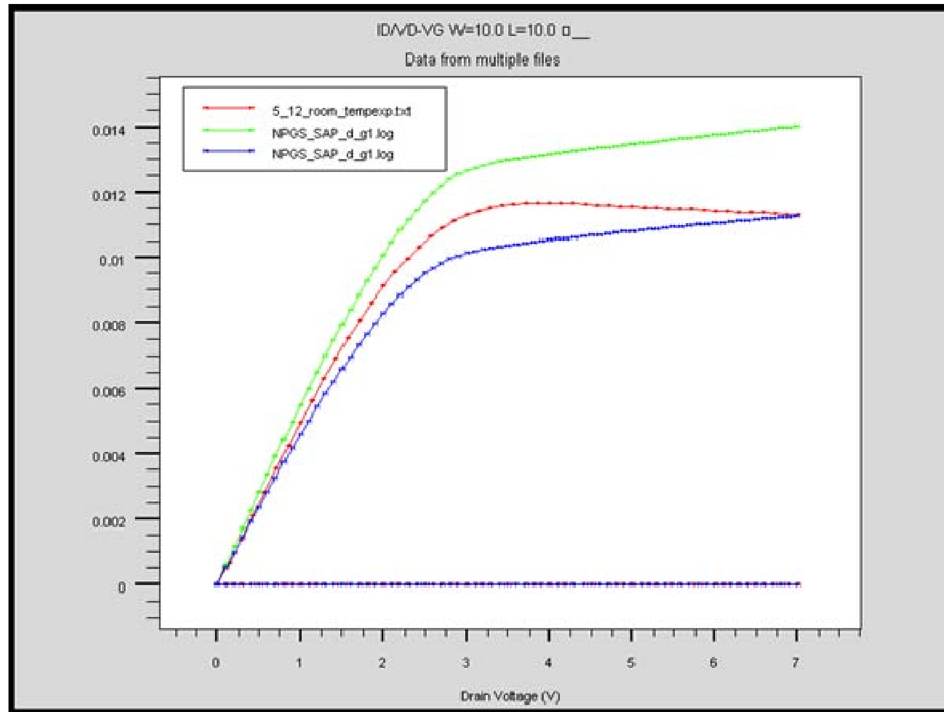

Figure 17. I(A)-V curves comparing actual vs. simulated device.

The simulation of the self heating effects is compared to the actual device at room temperature. Figure 18 shows the results for a gate voltage of -1 at the top and stepped down to -5 volts at the bottom. The red lines are the device measurements at the same gate bias. The thermal heating can be seen in Figure 19 with a peak temperature of 405º Kelvin. The picture shows the peak temp at the drain side of the gate which agrees with the results from Freeman [23].

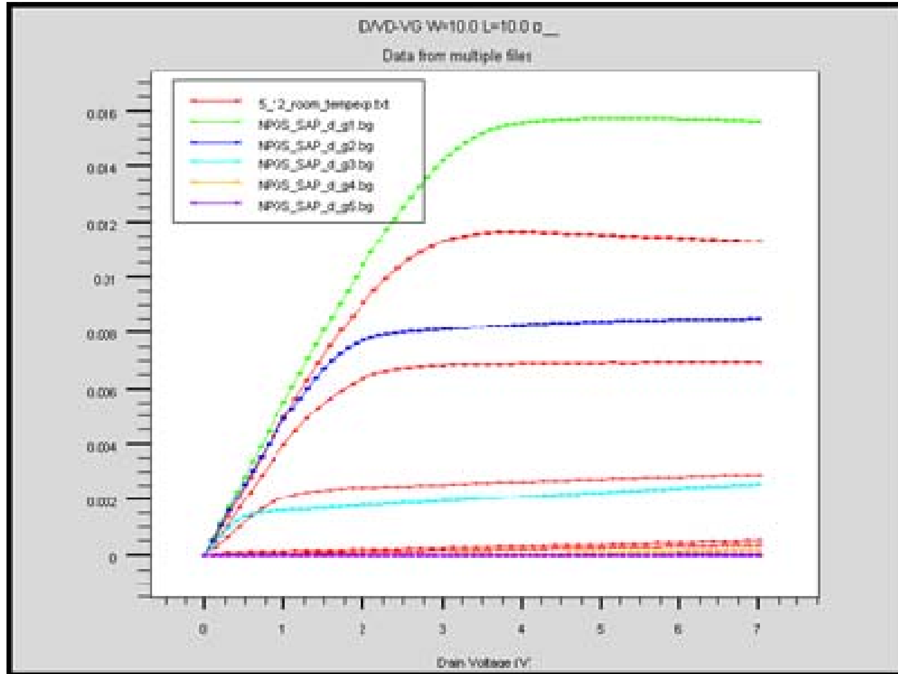

Figure 18. 2D Model Room Temperature I(A)-V simulated and actual (RED).

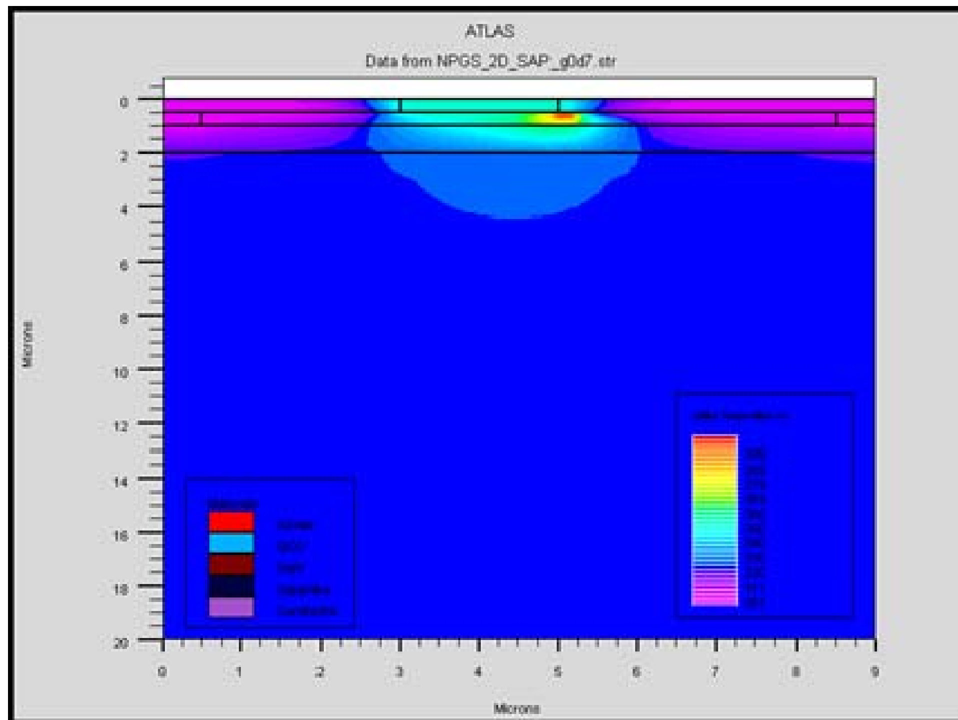

Figure 19. 2D Model Lattice temperature plot for room temp simulation. Peak temperature 399º Kelvin.

The simulated device for the room temperature curve did correlate to measurements. The next set is the 400º Kelvin and 500º Kelvin simulation curves that validated actual device measurements. Figure 20 shows the resulting simulated I-V for the gate bias at -1 volt compared to measurements at 400º Kelvin and 500º Kelvin. Several more runs were conducted and matched to various gate bias and temperature conditions. The dark blue line is the simulated device being compared to the red line of the actual device at 400º Kelvin. The light blue line is the simulated device being compared to the green line of the device at 500º Kelvin. The results match to less than a ten percent difference on the 400º Kelvin and 500º Kelvin curves.

The simulated results correlate well with the UC Berkeley device measurements except that the room temperature curves do not match unless the simulation is run at 50º Kelvin above room temperature. This could be attributed to the possibility of not allowing the device to cool properly between measurements. This also could be due to not knowing the exact thermal barrier that existed between the device and the hot chuck. With the model set in two dimensions the simulation was then converted to three dimensions.

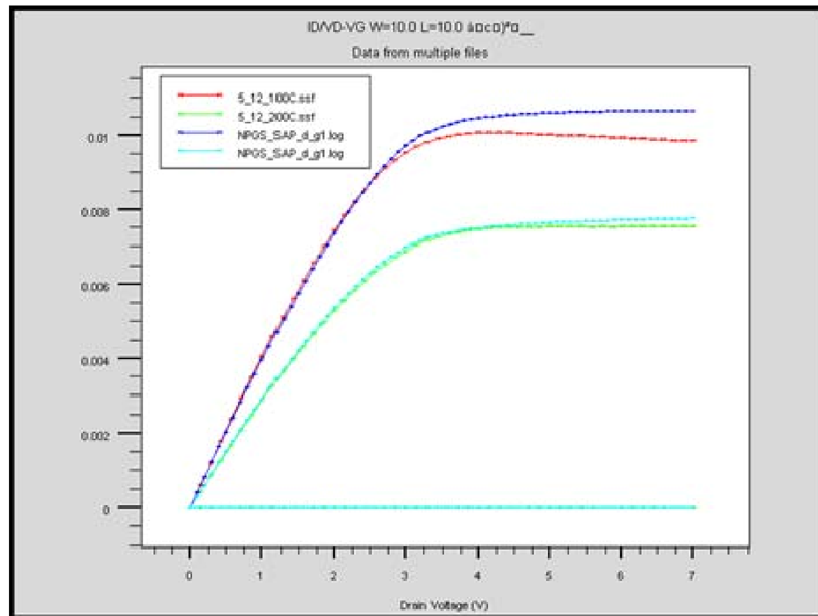

Figure 20. 2D Model I(A)-V comparison at 400º and 500º Kelvin.

3. Comparison of a 2D to 3D Model

The model was changed to include the z-axis component to make a one hundred micron width. The mathematical solver method also had to be changed from BLOCK to NEWTON, since BLOCK does not work in 3D. The 3D model run could not find convergence with a solution, which resulted in an errors and aborted runs. The LOG file output was a short amount of data, but contained enough information to see high current values and large temperature jumps that would lead to a convergence issue. The contact resistance was then changed due to initial input in 2D is in units of Ω-cm^2 and the 3D system uses units of Ω-cm^3. The model was run with the implemented change to the contact resistance which produced the same error. The 2D modeling system resulted in the current being limited using a contact resistance and the 3D system showed no effect from a contact resistance value. The resistance was then changed to a lump input resistance, which had no effect on the 3D model run.

The inability to get a convergence was due to a high temperature variations from the high current. This result led to the need to reduce the channel current. This was done by returning to Newham's [7] method of changing Albrecht's constants to lower the mobility to a desirable value. The mobility was lowered by one third by multiplying each constant a, b, and c by three. The thermal conductivity for the GaN layers was returned to the default values and the sapphire thermal conductivity was set to 32 W/m-K. The 3D model was then successful. This was then compared to the 2D results at the -1 volt gate bias and at room temperature. Figure 21 shows the comparison of the I-V curves for the 2D (green) and the 3D (red) models. The result is a 50% difference in the drain current which needed resolution.

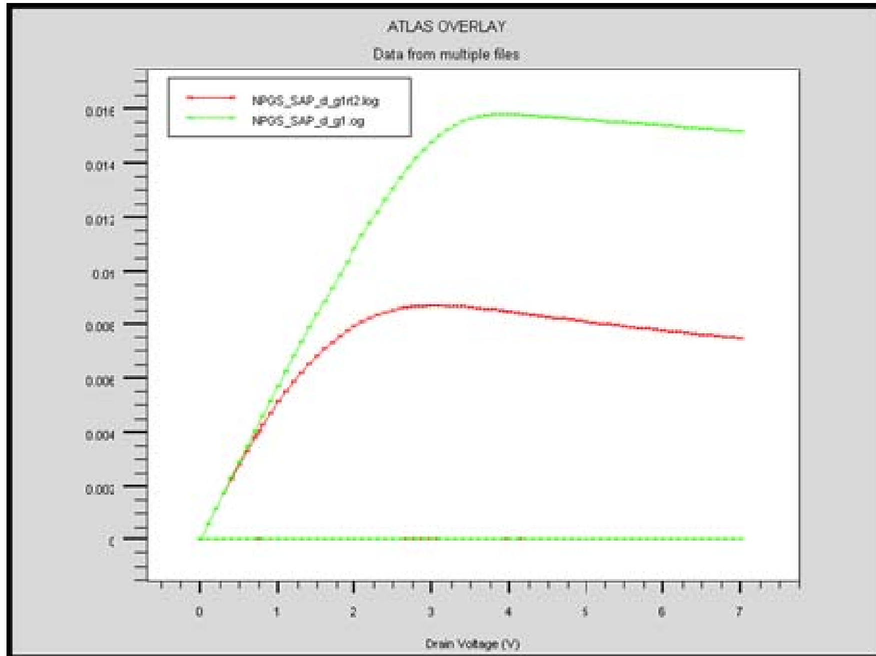

Figure 21. Comparison of I(A)-V curves for 2D and 3D model.

The first thing examined was the difference in the numerical solver used between the two models, the 2D using Block and the 3D using Newton. The 2D model was then changed to use Newton as the solver. The result was an instability in the Newton solver in the 2D model used. Figure 22 shows the I-V curves for the 2D model using Block (red) and Newton (green) solvers. Figure 23 shows the global device temperature differences between Block (red) and Newton (green). These results show a divergence between the two models and that the Newton method having a temperature heating to 750º Kelvin is not realistic.

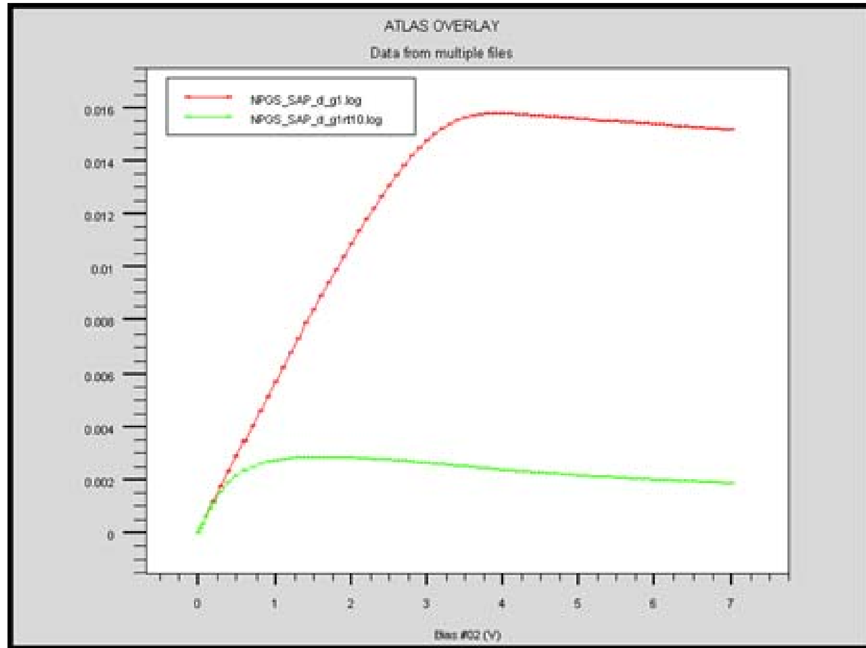

Figure 22. Comparison of I(A)-V curves for Block and Newton solver.

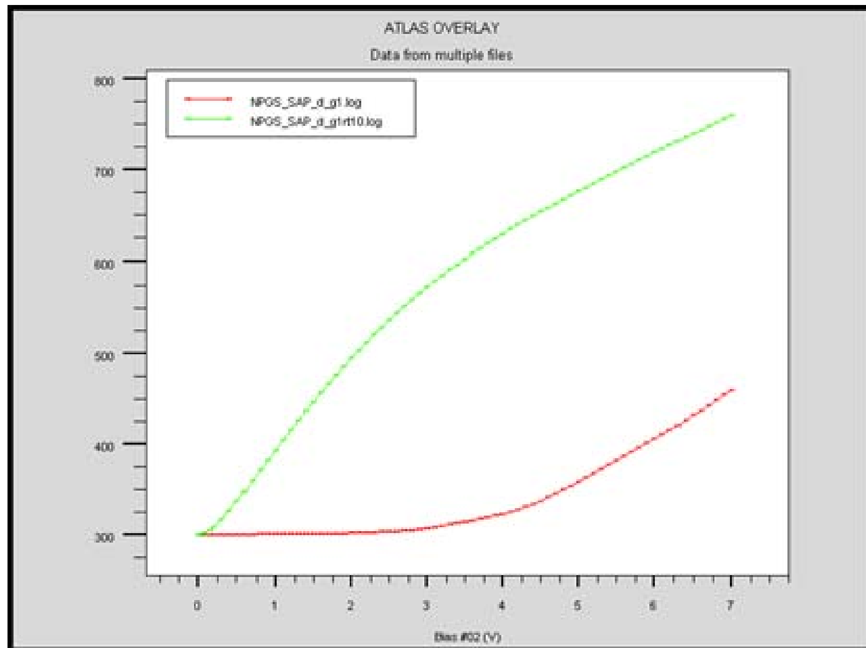

Figure 23. Comparison of global device temperature (K) for Block and Newton solvers.

This was now looked at as in issue that may affect the 3D modeling, since the Block solver is not incorporated into BLAZE3D™. This led to consulting with Robin Jones at Silvaco International, to be able to determine the differences. The problem that was occurring in the 2D was due to using a non-isothermal model. It is recommended to use the Block solver for non-isothermal models in 2D. The recommended solver for the 3D model was a Block iterative implemented by using BICGST in the method statement. The effect of running non-isothermal models was done in order to verify the same results could be received in 2D and 3D.

The 2D and 3D models were converted to isothermal models by removing the LAT.TEMP from the model statement. The Models used the same values for the Albrecht's equation that had a multiplication factor of 3 times for the Albrect's constants. The results include I-V curves for both Newton and Block solvers in 2D. This same result was seen for the I-V curve produced by the 3D model. Figure 24 shows the matching I-V curves for the isothermal models. This result shows that the solvers are comparable for a 2D model and a 3D model without any heating effects being accounted for and the same thermal constants.

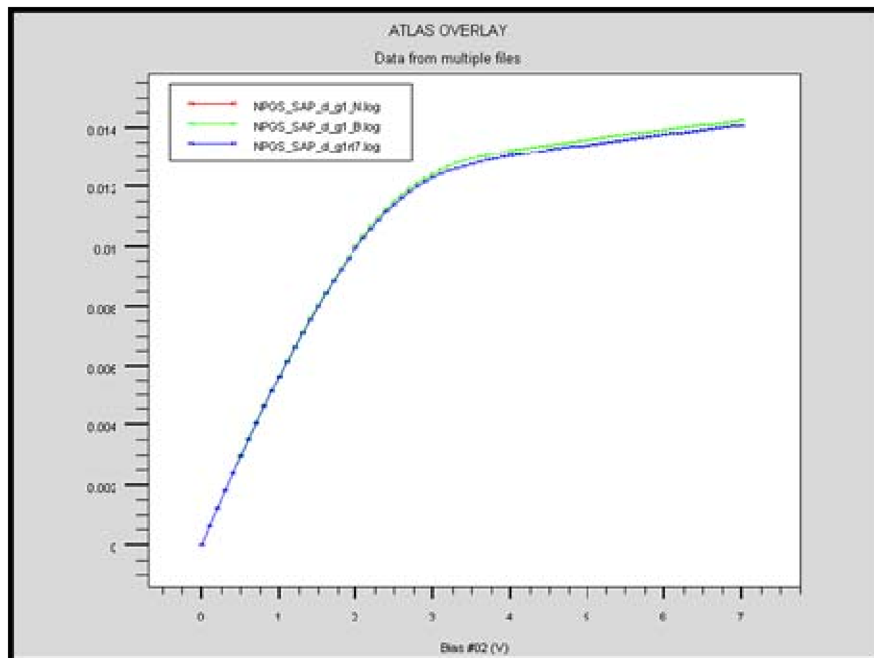

Figure 24. Comparison of isothermal models for 2D and 3D.

The previous results of the 3D model with the heating effects compared to the 2D show an increase in self-heating effects. The results of the 3D model for the heating effects generated in the GaN device are similar to with the results from Freeman [23] and McAlister [22]. The manipulation of changing the thermal constants that was done for 2D was not needed for 3D. This work uses the results from the 2D best match for the UC Berkeley device to develope a best fit 3D model.

The I-V characteristic curves were used to make the comparison between 2D and 3D. Changes to the Albrecht's constants were made in the 3D model until the best match was achieved. This was done by using the same multiplication factor for each of the Albrecht's constant. The best fit 2D model was run with the thermal properties removed and the results were compared to the 3D runs. Several comparisons were done with the best fit 2D to a 3D model with an altered Albrecht's constants; it was found that using a multiplication factor of 2.4 times the constants was required to fit. The best fit matched I-V curves between 2D and 3D is shown in Figure 25. This set of constants will be used for the rest of the modeling in 3D for this thesis. The results of the thermal 3D modeling will be looked at next.

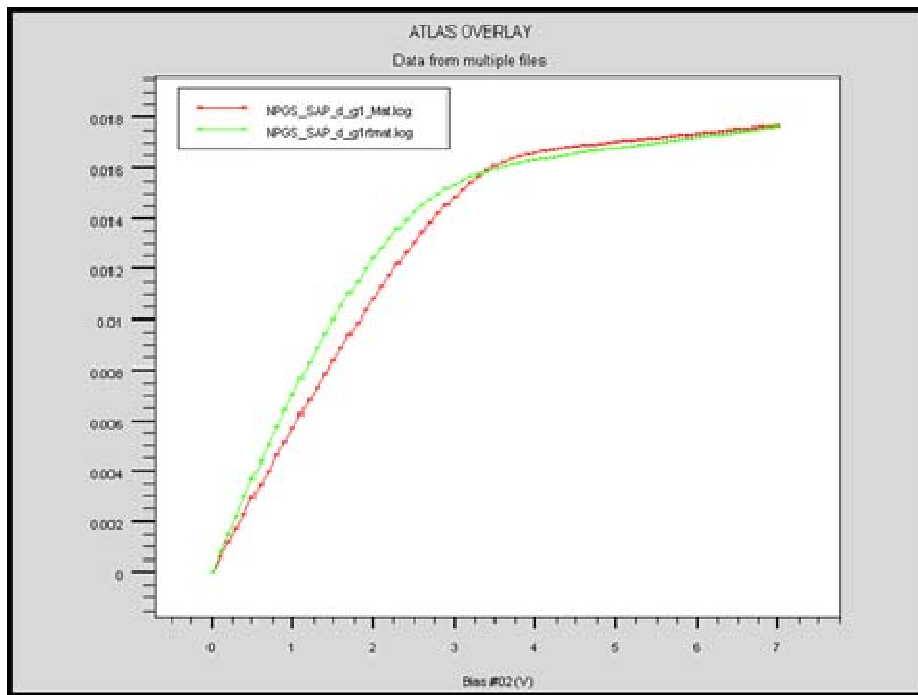

Figure 25. Best match for 2D and 3D I(A)-V curves

The heating effects of the device can be seen in the I-V characteristic curves shown in Figure 26. This is similar to the heating effects seen in the actual device I-V characteristic curves. This shows that as the average channel temperature increases the mobility will decrease resulting in a lower current. This is the same result that was shown by Freeman [23] and McAlister [22]. The isothermal model curve is shown in red, the thermal model curve is shown in green, and the actual device curve is shown in blue.

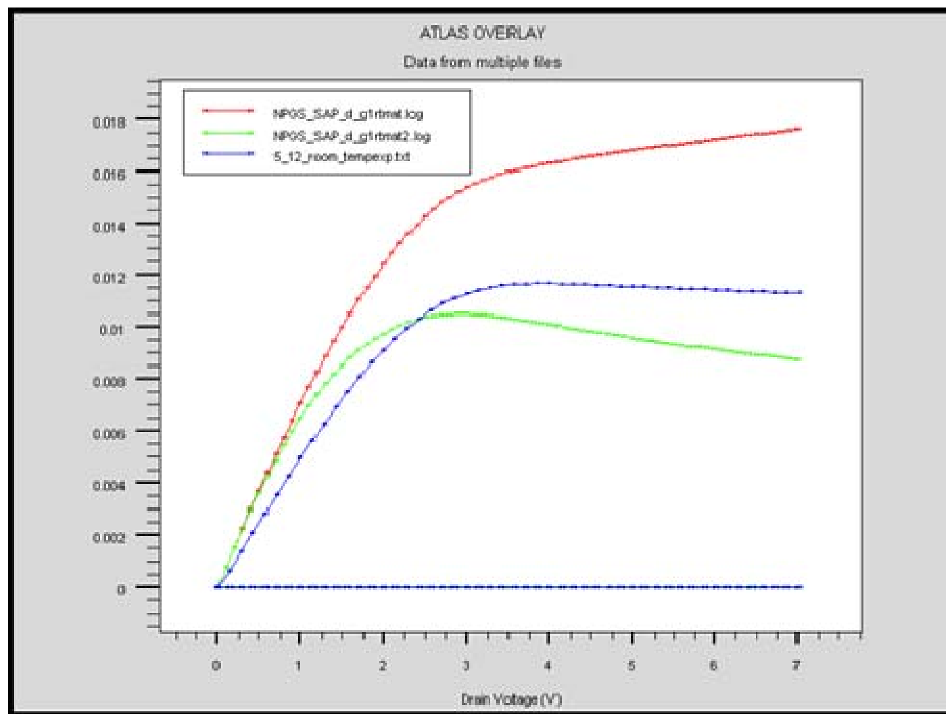

Figure 26. Comparison of the thermal model and isothermal model I(A)-V curves.

The thermal picture for the 3D is shown in Figure 27. This shows the thermal heating gradient from the channel to the substrate. The temperature range was 392º K (red) to 300º K (blue). The heat production on the drain side of the gate is shown in Figure 28. The passivation oxide layer was hidden to be able to view this better.

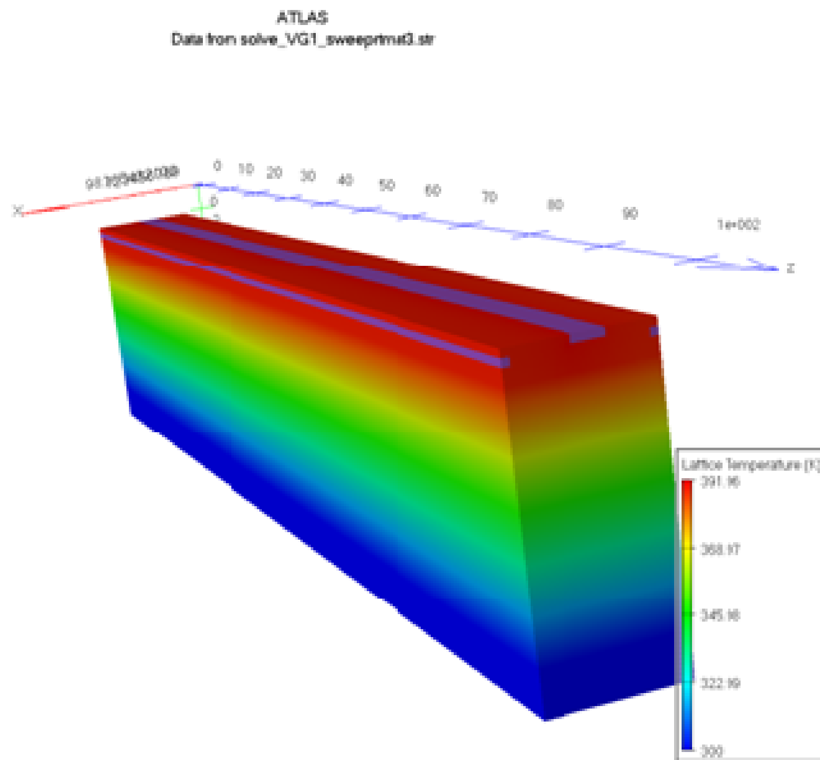

Figure 27. 3D thermal model results. Red at 392º K to Blue at 300º K

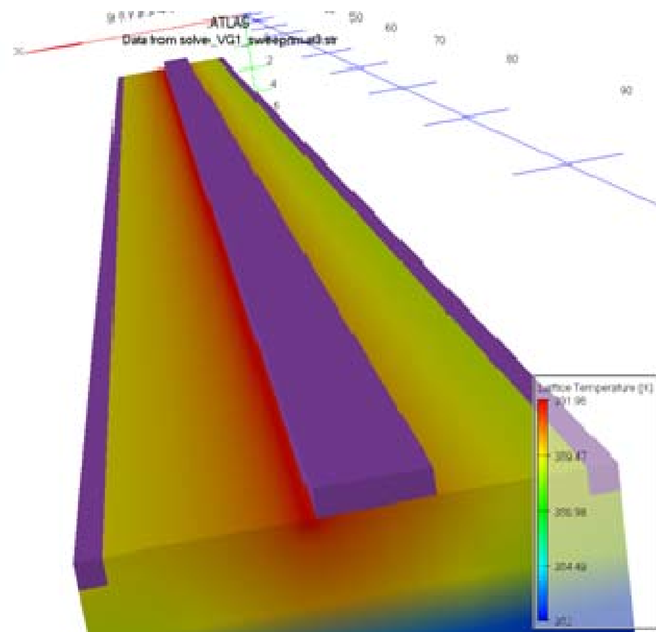

Figure 28. 3D heating in channel under the gate. Red at 392º K

The device modeling can allow for other device characteristics to be looked at in 2D or 3D. Figure 29 shows the electron concentration in 3D the red plane is the 2DEG discussed in Chapter II. The 3D output was then converted to 2D TONYPLOT^{TM} to be able to extract information. Figure 30 shows the thermal heating in the middle of the device in 2D. Figure 31 shows the temperature profile of the device through the channel. The peak temperature in the device is 92º K above room temperature.

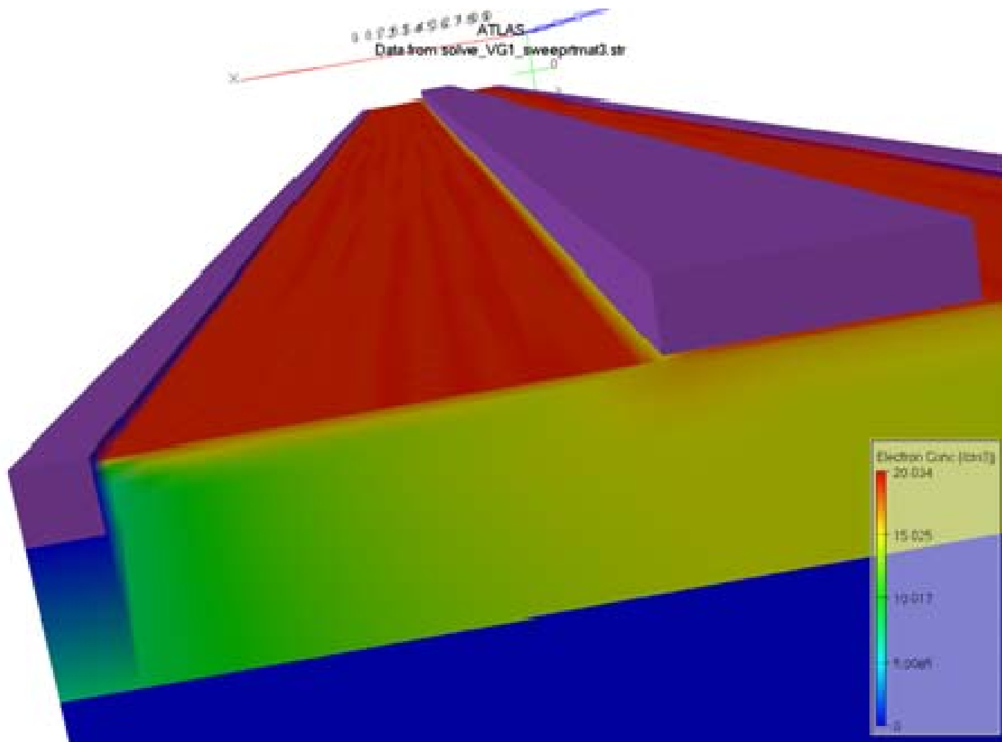

Figure 29. 3D electron concentration

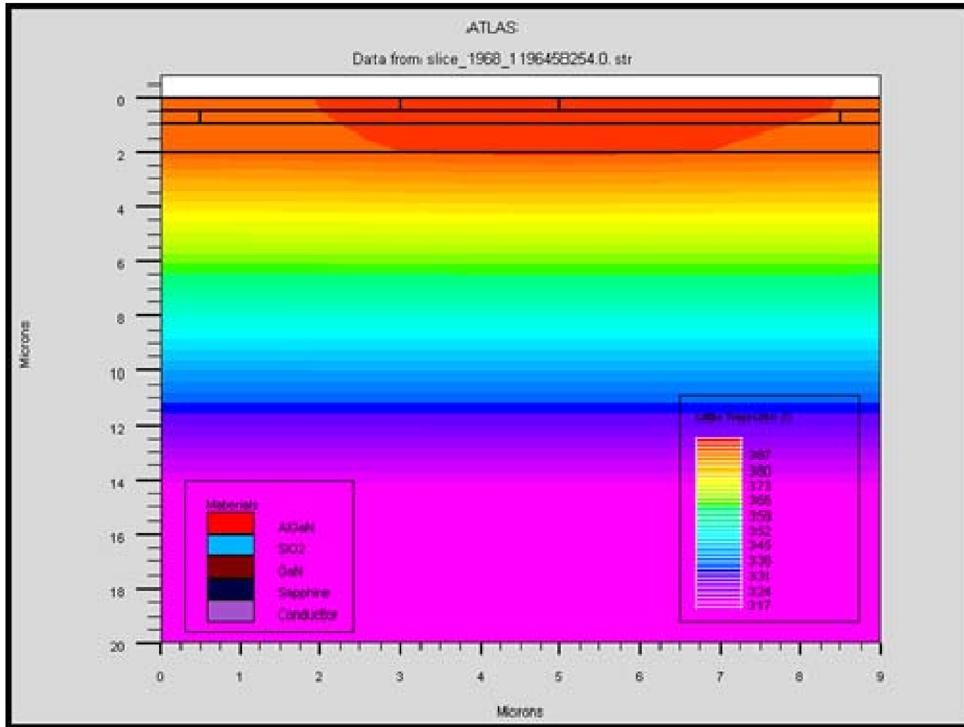

Figure 30. 2D thermal image from middle of the device.

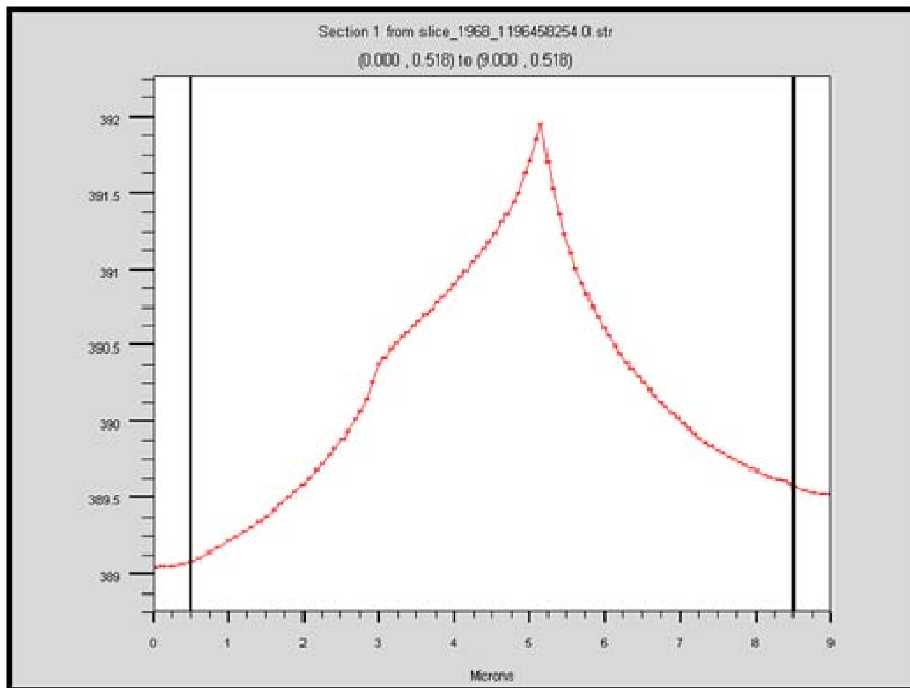

Figure 31. Temperature (K) profile of the device across the channel.

B. MODELING HEMT ON DIAMOND

1. Changes to Model for Diamond Substrate

The investigation to use the 3D system to model a diamond substrate was done by direct substitution. The actual substrate was not manufactured and will be left to model as further work. The sapphire in the material statement was changed to diamond and this was left as an insulator. This was so the electrical properties of the diamond would not be calculated in the model run. The thermal constant used for this model was 12 W/cm-K from the data from SP3 [13]. This was inserted into the model by changing TC.A to 0.083 in the material statement. The final 3D model is shown in Appendix C. The results from this model are shown in the next section.

2. Comparison of Diamond and Sapphire Substrate

The results show the effect of heat removal from the channel of the device and the improved I-V characteristics. Figure 32 shows the I-V curve comparison between the sapphire (red) and the diamond (green) substrate 3D models. The global device temperature was approximately 86º K lower for the diamond substrate. This is the expected result since the thermal conductivity of diamond is 40 times greater than sapphire. The global device temperature comparison is shown in Figure 33 showing sapphire (red) and the diamond (green).

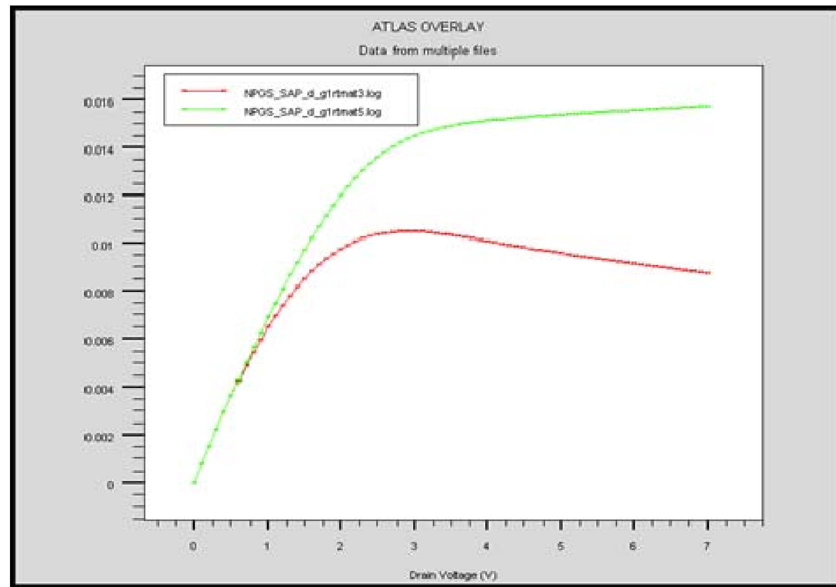

Figure 32. Comparison diamond and sapphire substrate I(A)-V curves

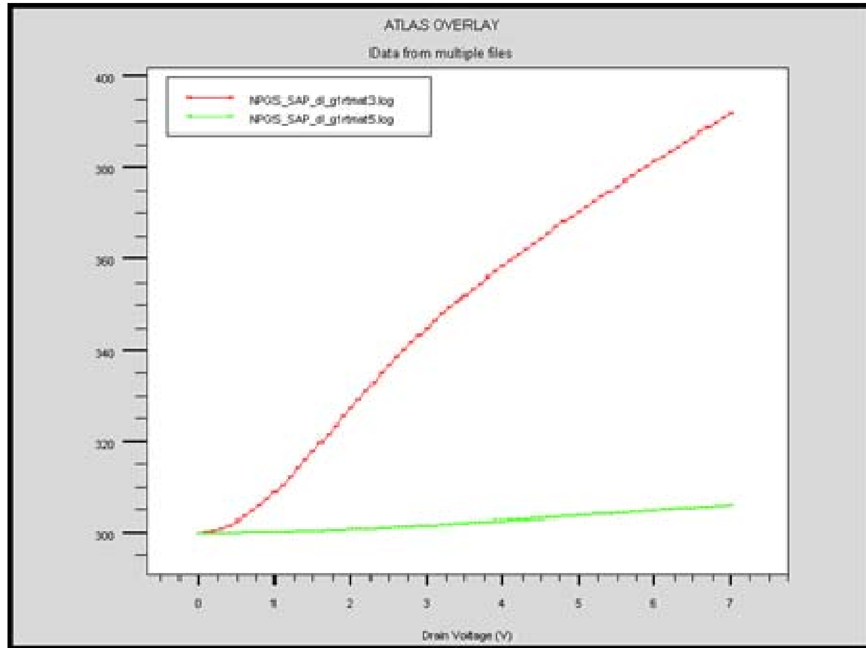

Figure 33. Comparison of global device Temperature (K).

The source of the heating was still at the drain side of the gate. Figure 34 shows the thermal heat dissipation through the material. Figure 35 show the temperature profile across the channel of the device. The channel temperature is lower resulting in a higher drain current than the sapphire substrate device. The electric field peak occurs at the drain side of the gate. The electric field profile is shown in Figure 36. The peak self-heating is occurring at the same place as the peak electric field.

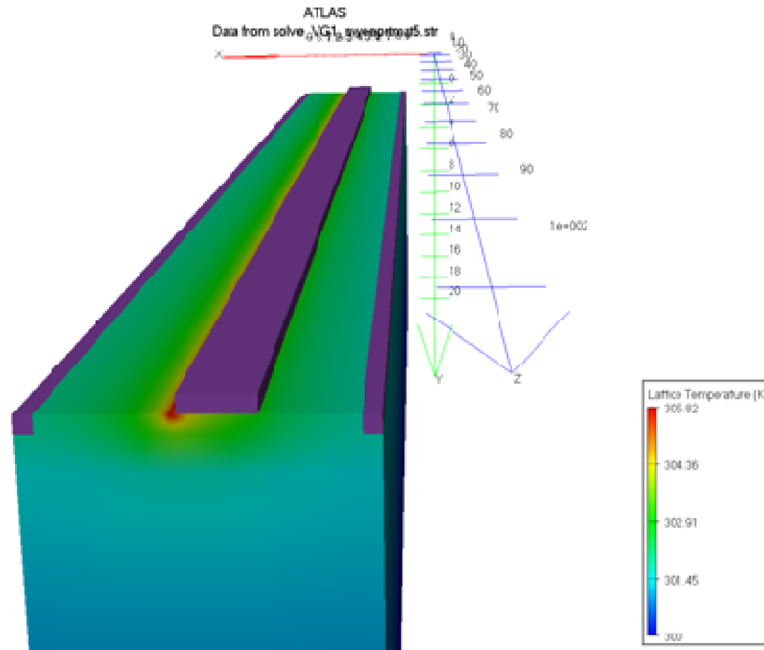

Figure 34. Thermal image of diamond substrate HEMT.

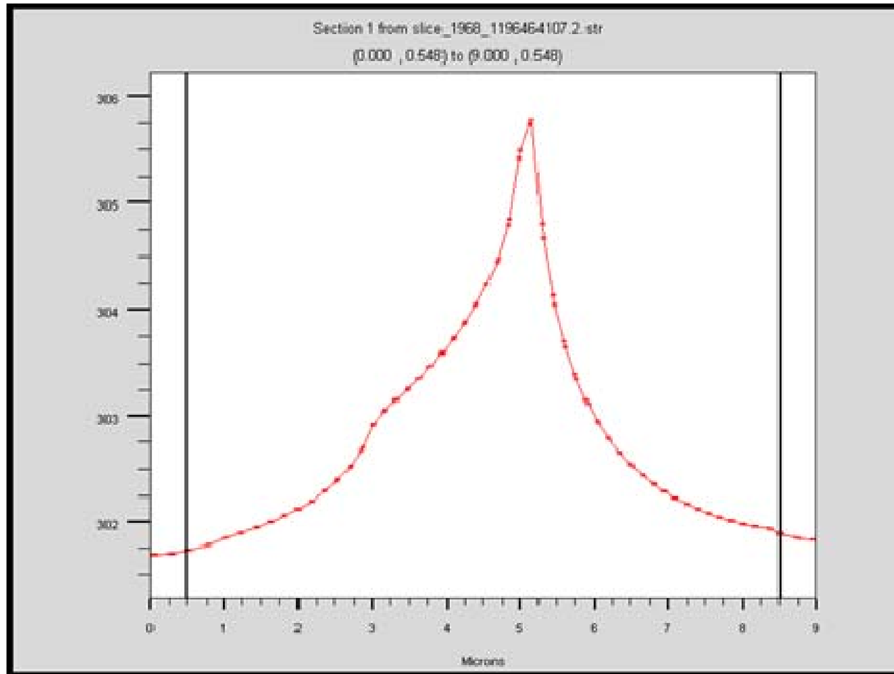

Figure 35. Diamond substrate model channel temperature profile.

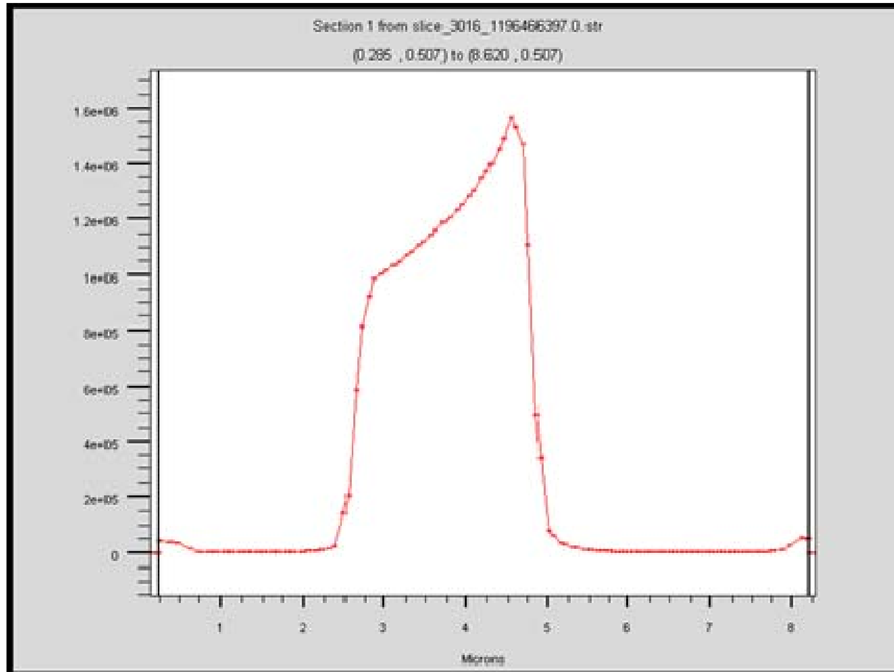

Figure 36. Electric field profile across channel

THIS PAGE INTENTIONALLY LEFT BLANK

IV. CONCLUSIONS AND RECOMMENDATIONS

A. CONCLUSIONS

This thesis showed the effectiveness of modeling GaN HEMTs in 2D and 3D using the Silvaco software package. The 2D modeling showed a better predictive ability for I-V characteristics. The 3D modeling better showed the actual thermal effects that are occurring in a GaN device. Though the actual device temperatures were not measured, the thermal heating effects are seen in the I-V curves with the negative slope at the end of the drain current curve. Through the comparison of several model runs and the testing of the actual device, this thesis was able to produce a suitable 3D model for a GaN HEMT.

The issues in this thesis were mainly seen when switching from a 2D model to a 3D model. The matching of the 2D model was easily done based on the data of the actual device. The 3D model was harder to match due to the time it took to run a simulation. There was an increase of about six to ten times longer than the 2D counterpart. The lack of understanding of the operation of the different numerical solvers available in the ATLAS program resulted in process slowdown. The other issue that could not be resolved was the impact of contact resistance in the 3D model.

The effects of self-heating and thermal dissipation were key focuses for this thesis. The operation of the device is clearly effected by the average channel temperature. This was shown in Albrecht's equation and in the 3D modeling. The effects of thermal dissipation can be seen with the change of the substrate. The temperature in the device with sapphire substrate was modeled with resulting peak of 392º Kelvin. The temperature in the device with a diamond substrate was modeled with resulting peak temperature of 306º K. The results of the modeling show that improved thermal conductivity of a substrate can lead to improved operational performance of the device.

The improvement in temperature can be related to improved reliability. The Arrhenius equation correlates the failure rate to temperature in electronic components. Equation (5) is the Arrhenius equation used to solve for failure rate. The activation energies of 1.70 eV and 1.05 eV are used. The value of 1.70 eV was obtained from the

work of S. Singhal et al. [24]. The value of 1.05 eV was chosen for being common to most semiconductor devices. The equation was solved using the final simulated temperatures for the 3D models of the device on diamond and sapphire. The result of the calculation is an increase in mean time to failure (MTTF) by 6000 to 1e6 times for the device on diamond.

$$R = Ae^{-\frac{E_a}{kT}} \tag{5}$$

Where; R is the failure rate, A is the empirical rate constant, E_a is the activation energy (eV), k is Boltzmann's constant (8.62e-5 eV/K), T is the temperature (K).

This thesis was successful in showing the modeling of the operation of GaN HEMTs in both 2D and 3D. The comparison of the two different modeling techniques showed advantages and disadvantages of each. The 3D modeling is more accurate when incorporating thermal heating effects. This also shows that with improved thermal management GaN may be seen as a future substitute for high power RF TWTs.

B. RECOMMENDATIONS

The modeling that was done for this thesis incorporated a direct switch from a sapphire substrate to a diamond substrate. This is not what is actually being produced for GaN substrates. Naval Postgraduate School is working with the SP3 Company that is producing a diamond substrate for GaN devices. This substrate is created on a silicon wafer which is then etched to less than two microns thick. The GaN will then be grown on top of the silicon that was left in place. The future modeling needs to incorporate this silicon layer to see how the thickness of this layer will affect thermal dissipation. Figure 37 shows SP3's layout of the proposed diamond substrate [13].

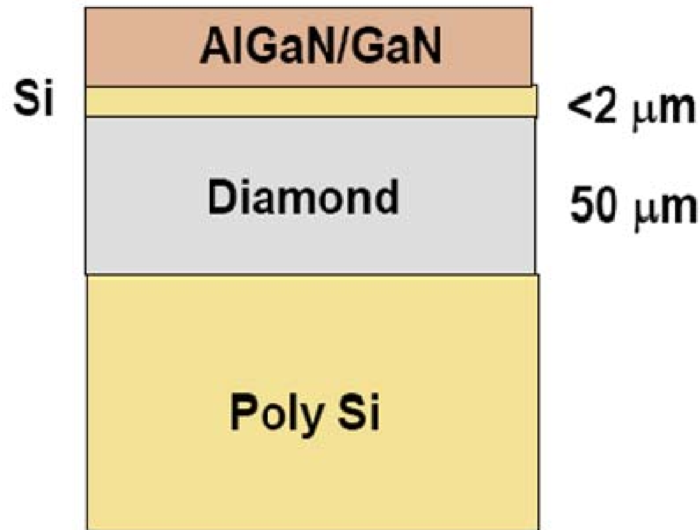

Figure 37. GaN on Diamond Proposed by SP3 From [13].

The eventual results from Air Force Research Lab's (AFRL) testing of a device manufactured using SP3's substrate should be used as another comparison for modeling. If possible, thermal information should be obtained as another means of verification of model operation. Future modeling should be done in 3D due to better incorporation of self-heating and thermal effects. The results should also be compared to those of Felbinger [25] who also tested GaN on Diamond substrate. The bonding process used for Felbinger's experiments was different than that being done by SP3. The effect of the different processes on the piezoelectric polarization should be looked at to help determine the interface charge.

The different numerical solvers should be looked at more closely to ensure the proper method is being used. Also the different parts of the thermal equation should be looked at closely to ensure those effects are properly modeled for GaN HEMT. The incorporated functions for GaN are very useful; it is not clear how some of the standard functions interact with GaN specific functions. Future modeling should use the functions that the Silvaco software package has developed for GaN. The data for the UC Berkeley device could also be improved by mounting the device onto a thermal heat sink. This will allow for more accurate measurements to compare to the model.

THIS PAGE INTENTIONALLY LEFT BLANK

LIST OF REFERENCES

[1] Electronics Manufacturing Productivity Facility, ONR, http://www.empf.org, July 2007.

[2] D. Love, "Value Engineering in the Lean Environment," *2007 Government Value Management Conference*, Houston, 2007.

[3] R. T. Kimerley, H. B. Wallace, and M. N. Yoder, "Impact of Wide Bandgap Microwave Devices on DoD Systems," *Proceedings of the IEEE*, Vol. 90, NO.6, pp. 1059-1064, June 2002.

[4] M. Sugimoto, H. Ueda, T. Uesugi, and T. Kachi "Wide-Bandgap Semiconductor Devices for Automobile Applications," *Toyota Central R&D Labs*, CS MANTEC Conference, April 2006.

[5] J. C. Freeman, "2003, Basic Equations for the Modeling of Gallium Nitride (GaN) High Electron Mobility Transistors (HEMTs)." *NASA/TM--2003-211983* http://gltrs.grc.nasa.gov/reports/2003/TM-2003-211983.pdf, November 2007.

[6] R. P. Salm, "Thermal Modeling of GaN HEMTs on Sapphire and Diamond." *Master's Thesis,* Naval Postgraduate School, Monterey, California, 2005. [Electronic].

[7] W. S. Newham, "Development of AlGaN/GaN High Electron Mobility Transistors (HEMTs) on Diamond Substrates." *Master's Thesis*, Naval Postgraduate School, Monterey, California, 2006. [Electronic].

[8] S. Tzeng, "Low-Frequency Noise Sources in III-V Semiconductor Heterostructures," University of California, Berkeley, 2004.

[9] Microsystem Technology Office, DARPA, http://www.darpa.mil/MTO/Programs/wbgsrf/index.html, August 2007.

[10] National Compound Semiconductor Roadmap, ONR, http://www.onr.navy.mil/sci_tech/31/312/ncsr/materials/default.asp, November 2007.

[11] Parvesh Gangwani, Sujata Pandey, Subhasis Haldar, Mridula Gupta, R.S. Gupta, "Polarization dependent analysis of AlGaN/GaN HEMT for high power applications," *Solid-State Electronics* 51, pp. 130–135, 2007.

[12] Vargaftman, J. Meyer, L. Ram-Mohan,"Band Parameters for III-V Compound Semiconductors and their Alloys," *Journal of Applied Physics*, volume 89, number 11, pp. 5815-5875, June 2001.

[13] SP3 Incorporated, http://www.sp3inc.com/, November 2007.

[14] C. Kisielowski, “ Strain in GaN Thin Films and Heterostructures,” *Semiconductors and Semimetals*, Volume 57, pp 275-317, 1999.

[15] C. Kisielowski, J. Kruger, M. Leung, R. Klockenbrink, H. Fujii, T. Suski, “Orgin of strain in GaN thin Films,” *Proceedings of the 23rd Iinternational Conference on the Physics of Semiconductors*, Singapore, 1996

[16] N.Maeda, T. Nishida, N. Kobayashi and M. Tomizawa “Two dimensional electron gas density in $Al_xGa_{1-x}N$/GaN heterostructure field effect transitors,” *Applied Physics Letters*, Volume 73, Number 13, pp. 1856-1858, September 1998

[17] M. Mastro, J. LaRoche, N. Bassim, C. Eddy Jr., “Simulation on the effect of non-uniform strain from the passivation layer on AlGaN/GaN HEMT,” *Microelectronics Journal 36*, pp. 705-711, 2005

[18] O. Ambacher et al., “Pyroelectric properties of Al(In)GaN/GaN hetero and quantum well structures,” *Journal of Physics Condensed Matter*, vol. 14, pp. 3399–3434, 2002.

[19] Bernardini and V. Fiorentini, “Spontaneous Polarization and Piezoelectric Constants of III-V Nitrides”, Phys. Rev. B Vol. 56, No. 16, 15, pp. 10024-10027, October 1997.

[20] J. D. Albrecht, P. P. Ruden, S. C. Binari, and M. G. Ancona, “AlGaN/GaN Heterostructure Field-effect Transistor Model Including Thermal Effects,” *IEEE Trans. Electron Devices*, vol. 47, pp. 2031–2036, November 2000.

[21] Silvaco International, “Silvaco International, ATLAS User’s Manual,” September 2007.

[22] S.P. McAlister, “The Peak and Average Temperature in a Self-Heated GaN HFET,” *Solid-State Electronics* 51, pp. 142-146, 2007.

[23] J. C. Freeman, “Channel Temperature Model for Microwave AlGaN/GaN HEMTs on SiC and Sapphire MMICs in High Power, High Efficiency SSPAs,” *NASA/TM--2004-212900,* http://gltrs.grc.nasa.gov/reports/2004/TM-2004-212900.pdf, November 2007.

[24] S. Singhal, T. Li, A. Hanson, R. Therrien, J. Johnson, W. Nagy, J. Marquart, P. Rajagopal, J. Roberts, E. Piner, I. Kizilyalli, and K. Linthicum, “Reliability of Large Periphery GaN on Si HFETs,” *Microelectronics Reliability 46*, 2006.

[25] J. G. Feldbinger, M. Chandra, Y. Sun, and L. Eastman, “Comparison of GaN HEMTs on Diamond and SiC Substrates,” *IEEE. Electron Device Letters*, 2007.

APPENDIX A. MATLAB CODE

```
% This code is for the ploting of Albrecht's equation
% Show the effect of changing temprature and Ionized donor
concentration
% Breaks down into parts for A, B, C constants.
clear all;
a=(2.61e-4);
b=(2.90e-4);
c=(1.7e-2);
Nb=1:15;
N=Nb.*1e16;
temp=300;
optemp=1065;
for i=1:15
   u(i)=1/(((a*N(i)/1e17)*(temp/300)^(-
3/2))*log(1+3*((temp/300)^2)*(N(i)/1e17)^(-
2/3))+(b*(temp/300)^(3/2))+(c/(exp(optemp/temp)-1)));
end
plot(N,u)
ylabel('Mobility, cm^2/V/sec')
xlabel('Ionized Donors, /cm^3')
N2=1e16;
t2=300:5:350;
for i=1:11
     u2(i)=1/(((a*N2/1e17)*(t2(i)/300)^(-
3/2))*log(1+3*((t2(i)/300)^2)*(N2/1e17)^(-
2/3))+(b*(t2(i)/300)^(3/2))+(c/(exp(optemp/t2(i))-1)));
end
figure (2)
plot(t2,u2)
ylabel('Mobility, cm^2/V/sec')
xlabel('Temperature, K')
a2=1:100;
at=a2.*1e-5;
for i=1:11
      u3(i)=1/(((a*N2/1e17)*(t2(i)/300)^(-
3/2))*log(1+3*((t2(i)/300)^2)*(N2/1e17)^(-2/3)));
end
figure (3)
plot(t2,u3)
ylabel('Mobility, cm^2/V/sec')
xlabel('Temperature, K')
b2=1:100;
bt=b2.*1e-5;
for i=1:11
        u4(i)=1/(b*(t2(i)/300)^(3/2));
end
figure (4)
plot(t2,u4)
ylabel('Mobility, cm^2/V/sec')
xlabel('Temperature, K')
c2=.1:.1:10;
ct=c2.*1e-2;
for i=1:11
```

```
        u5(i)=1/(c/(exp(optemp/t2(i))-1));
end
figure (5)
plot(t2,u5)
ylabel('Mobility, cm^2/V/sec')
xlabel('Temeprature, K')
```

APPENDIX B. DECKBUILD CODE FOR 2D MODEL

```
######################################################################
######################################################################
#NPSG AlGaN/GaN HEMT Design
#
# 267 Angrstrom AlGaN layer
# Schottky WF=4.3
# GaN AlGaN
# Interface charge=.93e13
# no doping in algan
# Albrct mobility model
#######################################################################
go atlas
# Sweep increment
set vstart = 0
set vstop = 7
set vinc = .1
#################### Mesh Construction #############
####Mesing and width = 100 microns#################
mesh auto width=100
x.m l=0.0 s=0.25
x.m l=0.5 s=0.2
x.m l=1.0 s=0.2
x.m l=3 s=0.15
x.m l=5 s=0.15
x.m l=8 s=0.15
x.m l=8.4 s=0.2
x.m l=8.5 s=0.25
x.m l=9 s=.25
y.m l=0 s=0.25
y.m l=0.4 s=0.2
y.m l=0.5 s=0.005
y.m l=0.525 s=0.005
y.m l=0.5267 s=0.00002
y.m l=0.5269 s=0.00002
y.m l=0.5270 s=0.005
y.m l=0.6 s=0.05
y.m l=0.7 s=0.1
y.m l=1.0 s=0.2
y.m l=2.0 s=1
y.m l=3.0 s=3
y.m l=20 s=3
######################## Region Definitions ################
region num=1 x.min=0.5 x.max=8.5             y.max=0.5267 mat=AlGaN
x.comp=0.28
region num=2 x.min=0.0 x.max=9.0 y.min=0.0    y.max=0.5    mat=oxide
region num=3 x.min=0.5 x.max=8.5 y.min=0.5267 mat=GaN
region num=4 x.min=0.5 x.max=8.5 y.min=0.5287 y.max=1.0    mat=GaN
region num=5 x.min=0.0 x.max=9.0 y.min=1.0    y.max=2.0    mat=GaN
region num=6 x.min=0.0 x.max=9.0 y.min=2.0    y.max=20.0   mat=Sapphire


elec num=1 name=source x.min=0   x.max=0.5 y.min=0.5 y.max=1
elec num=2 name=drain  x.min=8.5 x.max=9   y.min=0.5 y.max=1
elec num=3 name=gate   x.min=3   x.max=5   y.min=0 y.max=0.5
elec num=4 substrate

############## Modifying Statements ##################
#######Inserts polarization effects#######
interface charge=9.3e12 y.min=.52 y.max=.5267 s.s
```

```
contact name=source con.resistance=5e-6
contact name=drain con.resistance=5e-6
contact name=gate work=4.3

mobility albrct.n
material mat=GAN TC.A=300
material mat=Sapphire TC.A=30 TC.B=.0156

models k.p print lat.temp joule.heat srh albrct temp=300

thermcontact num=1  y.min=19 y.max=20 temp=300 ^boundary alpha=1.7

output con.band val.band charge
method gumits=30 clim.dd=1e6 autonr block carr=1 NBLOCKIT=50
###################### Output Statements ##########
# idvd curves
solve
solve vdrain=0 vgate= -5
save outf=solve_vgate-5.str
log outf=NPGS_SAP_d_g5.log
solve name=drain vdrain=$vstart vfinal=$vstop vstep=$vinc
log off
solve vdrain=0 vgate= -4
save outf=solve_vgate-4.str
log outf=NPGS_SAP_d_g4.log
solve name=drain vdrain=$vstart vfinal=$vstop vstep=$vinc
log off
solve vdrain=0 vgate= -3
save outf=solve_vgate-3.str
log outf=NPGS_SAP_d_g3.log
solve name=drain vdrain=$vstart vfinal=$vstop vstep=$vinc
log off
solve vdrain=0 vgate= -2
save outf=solve_vgate-2.str
log outf=NPGS_SAP_d_g2.log
solve name=drain vdrain=$vstart vfinal=$vstop vstep=$vinc
log off
solve vdrain=0 vgate= -1
save outf=solve_vgate-1.str
log outf=NPGS_SAP_d_g1.log
solve name=drain vdrain=$vstart vfinal=$vstop vstep=$vinc
save outf=solve_VG1_sweep.str
log off
solve vdrain=0 vgate=0
save outf=NPGS_SAP_g0.str
log outf=NPGS_SAP_d_0.log
solve name=drain vdrain=$vstart vfinal=$vstop vstep=$vinc
save outf=NPGS_2D_SAP_g0d7.str
log off
quit
```

APPENDIX C. DECKBUILD CODE FOR 3D MODEL

```
######################################################################
######################################################################
#NPSG AlGaN/GaN HEMT Design
#
# 267 Angrstrom AlGaN layer
# Schottky WF=4.3
# GaN AlGaN
# Interface charge=.93e13
# no doping in algan
# Albrct mobility model
#######################################################################
go atlas
# Sweep increment
set vstart = 0
set vstop = 7
set vinc = .1
#################### Mesh Construction #############
####Mesing and width = 100 microns#################
Mesh THREE.D
# x plane meshing
x.m l=0.0 s=0.25
x.m l=0.5 s=0.2
x.m l=1.0 s=0.2
x.m l=3 s=0.15
x.m l=5 s=0.15
x.m l=8 s=0.15
x.m l=8.4 s=0.2
x.m l=8.5 s=0.25
x.m l=9 s=.25

# y plane meshing
y.m l=0 s=0.25
y.m l=0.4 s=0.2
y.m l=0.5 s=0.005
y.m l=0.525 s=0.005
y.m l=0.5267 s=0.00002
y.m l=0.5269 s=0.00002
y.m l=0.5270 s=0.005
y.m l=0.6 s=0.05
y.m l=0.7 s=0.1
y.m l=1.0 s=0.2
y.m l=2.0 s=1
y.m l=3.0 s=3
y.m l=20 s=3

# z plane meshing
z.m l=0.0 s=5
z.m l=100.0 s=5

######################## Region Definitions ################
region num=1 x.min=0.5 x.max=8.5             y.max=0.5267 z.min=0 z.max=100.0
mat=AlGaN   x.comp=0.28
region num=2 x.min=0.0 x.max=9.0 y.min=0.0    y.max=0.5    z.min=0 z.max=100.0
mat=oxide     insulator
region num=3 x.min=0.5 x.max=8.5 y.min=0.5267              z.min=0 z.max=100.0
mat=GaN      donors=1e15
region num=4 x.min=0.5 x.max=8.5 y.min=0.5287 y.max=1.0    z.min=0 z.max=100.0
mat=GaN
```

```
region num=5 x.min=0.0 x.max=9.0 y.min=1.0    y.max=2.0    z.min=0 z.max=100.0
mat=GaN       insulator
region num=6 x.min=0.0 x.max=9.0 y.min=2.0    y.max=20.0   z.min=0 z.max=100.0
mat=Diamond  insulator


elec num=1 name=source x.min=0   x.max=0.5 y.min=0.5 y.max=1 z.min=0
z.max=100.0
elec num=2 name=drain  x.min=8.5 x.max=9   y.min=0.5 y.max=1 z.min=0
z.max=100.0
elec num=3 name=gate   x.min=3   x.max=5   y.min=0 y.max=0.5 z.min=0
z.max=100.0
elec num=4 substrate

############## Modifying Statements ##################
#######Inserts polarization effects#######
interface charge=9.3e12 y.min=.52 y.max=.5267 s.s

#contact name=source resistance=5e-2
#contact name=drain resistance=5e-2
contact name=gate work=4.3

mobility albrct.n an.albrct=6.264e-4 bn.albrct=6.96e-4 cn.albrct=4.08e-2
#material mat=GAN TC.A=300 T1N=700
material mat=Diamond TC.A=0.083

models k.p print srh albrct temp=300 lat.temp joule.heat
thermcontact num=1  y.min=14 y.max=20 ext.temp=300 ^boundary alpha=1.7

output con.band val.band charge

method Bicgst
# NBLOCKIT=50 gumits=30 clim.dd=1e5 autonr newton carriers=1
###################### Output Statements #########
# idvd curves
solve
#solve vdrain=0 vgate= -3
#save outf=solve_vgate-3rt2.str
#log outf=NPGS_SAP_d_g3rt2.log
#solve name=drain vdrain=$vstart vfinal=$vstop vstep=$vinc
#log off
#solve vdrain=0 vgate= -2
#save outf=solve_vgate-2rt2.str
#log outf=NPGS_SAP_d_g2rt2.log
#solve name=drain vdrain=$vstart vfinal=$vstop vstep=$vinc
#log off
solve vdrain=0 vgate= -1
save outf=solve_vgate-1rtmat5.str
log outf=NPGS_SAP_d_g1rtmat5.log
solve name=drain vdrain=$vstart vfinal=$vstop vstep=$vinc
save outf=solve_VG1_sweeprtmat5.str
log off
#solve vdrain=0 vgate=0
#save outf=NPGS_SAP_g0rt2.str
#log outf=NPGS_SAP_d_0rt2.log
#solve name=drain vdrain=$vstart vfinal=$vstop vstep=$vinc
#save outf=NPGS_3D_SAP_g0d7rt2.str
#log off
quit
```

INITIAL DISTRIBUTION LIST

1. Defense Technical Information Center
   Ft. Belvoir, Virginia

2. Dudley Knox Library
   Naval Postgraduate School
   Monterey, California

3. Chairman, Code EC (590)
   Department of Electrical and Computer Engineering
   Naval Postgraduate School
   Monterey, California

4. Professor Todd R. Weatherford, Code EC(590)/Wt
   Department of Electrical and Computer Engineering
   Naval Postgraduate School
   Monterey, California

5. Andrew A. Parker, Code EC(590)/Pk
   Department of Electrical and Computer Engineering
   Naval Postgraduate School
   Monterey, California

6. Jerry Zimmer
   SP3 Diamond Technologies
   Santa Clara, California

7. Robin Jones
   Silvaco International
   Santa Cl Clara, California

8. LT William Gibson,
   United States Navy
   Monterey, California